CCFE
CULHAM CENTRE FOR FUSION ENERGY

UK Atomic Energy Authority

UKAEA-CCFE-CP(25)16

J. Emmerson, A. Shackleford, X. Lefebvre, R. Brown

Performing hydrogen permeation experiments for fusion applications

Performing hydrogen permeation experiments for fusion applications

J. Emmerson, A. Shackleford, X. Lefebvre, R. Brown

This paper has been submitted to
33rd Symposium on Fusion Technology (SOFT), Dublin, Ireland, 22 - 27 September 2024

Fusion Engineering and Design 220 (2025) 115351

Contents lists available at ScienceDirect

Fusion Engineering and Design

journal homepage: www.elsevier.com/locate/fusengdes

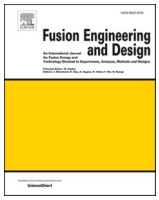

Tritium permeation experiments; design choices and appropriateness to fusion application research

Teuntje Tijssen *

United Kingdom Atomic Energy Authority, Culham Campus, Abingdon, OX14 3DB, United Kingdom

ARTICLE INFO

Keywords:
Tritium
Permeation
Hydrogen isotopes
Experimental verification

ABSTRACT

Tritium permeation is expected to be a major challenge in many locations in the fuel cycle of future fusion reactors. Countless permeation experiments have been performed trying to address this issue, each with their own characteristics including experimental conditions created, materials used, and detection methods employed. This paper reports the main outcomes of these past investigations, categorising them by their mode of operation rather than by the materials studied. The limitations of scientific experiments in recreating future conditions in fusion fuel cycles, and efforts to decrease this discrepancy, are discussed. Factors to consider when designing a permeation experiment and how these decisions affect the measurements that can be obtained are considered.

1. Introduction

Nuclear fusion reactors provide an enticing prospect of a clean, safe way of generating electricity, fuelled by unlimited resources. However, to realise this goal, there are several engineering challenges left to overcome. Most future fusion reactors are designed to use a 50:50 mixture of deuterium and tritium as fuel. Although deuterium is readily available through extraction from sea water, the use of tritium comes with several difficulties. Tritium is both scarce and radioactive, and as such needs to be contained to minimise losses to surrounding materials, systems, and the environment. Additionally, fusion reactors are required to breed tritium in breeder blankets to compensate for tritium being burned up and ensure self-sufficiency.

Reduced activation ferritic/martensitic (RAFM) steels are being considered as candidate structural materials for these breeder blankets, due to their excellent thermal and mechanical properties, such as low swelling and low radioactive activity after irradiation [1]. However, at the planned operating temperatures of the breeder blankets, approximately 500 °C, RAFM steels have a high permeability for tritium [2]. This alludes to large losses of tritium to the coolant due to the substantial amounts of tritium that are present in the breeder blankets.

Tritium permeation into the coolant is problematic for several reasons. Firstly, these losses impose high efficiency requirements onto purification systems to recover the tritium from the coolant. This is expected to require a lot of energy which reduces the net energy production of the fusion power plant. Furthermore, tritium permeation also reduces the net breeding ratio, imposing the need to install larger breeder blankets to counteract this. Besides loss of confinement, hydrogen permeation will cause embrittlement in structural materials. This can range from slow-strain rate embrittlement and delayed failure under stress, even after exposure to hydrogen at pressures as low as atmospheric, to bubble formation, leading to blistering, more common for high fugacity exposure [3,4]. And lastly, since the coolant carries heat away from the breeder blanket towards the steam generator used to generate electricity, there is a risk of tritium permeating through the heat exchanger into the steam generated and contaminating the environment [5].

The total EU DEMO tritium exhaust limit is estimated at 2 mg/day or 1 g/yr; [6,7]. In contrast, depending on the breeding blanket concept, tritium permeation from the blanket into the coolant has been estimated anywhere between 1 and 50 g/day [5,7]. Unfortunately, there is still much uncertainty about the solubility of tritium in materials such as eutectic lithium lead (LiPb), which leads to a variation in estimates of the calculated tritium losses up to 90 % [8].

These values demonstrate the considerable efficiency required for the coolant purification system. To reduce this need, coatings with a low permeability can be applied to the structural materials in the breeder blanket. Estimates suggest a Permeation Reduction Factor (PRF) between 100 – 1000 is needed in the breeder blanket [8,9] to reduce tritium permeation into the structural materials and to maintain a tritium concentration in the coolant that is low enough for the coolant purification system to process. Permeation barriers may also need to be

* Corresponding author.
E-mail address: Teuntje.tijssen@ukaea.uk.

https://doi.org/10.1016/j.fusengdes.2025.115351
Received 25 October 2024; Received in revised form 14 February 2025; Accepted 16 July 2025
Available online 24 July 2025

applied in the steam generator to further reduce tritium losses to the environment. Tritium permeation is not limited to breeder blankets; there are various other locations in the fusion fuel cycle where high concentrations of tritium occur at high temperatures. Anti-permeation coatings can provide the additional benefits of protection against corrosion from liquid LiPb and electrical insulation reducing magneto-hydrodynamic effects [2].

The aim of this paper is to provide insight into the operation of permeation experiments. First, the theory of hydrogen permeation through materials will be discussed (Section 2), followed by a consideration of candidate structural materials and anti-permeation coatings in Section 3. In Section 4 several factors that influence the permeation rate will be discussed, along with the limitations of existing scientific experiments to study these effects compared to the conditions under which permeation barriers will be applied. This is followed by a discussion of experiments performed with breeder materials, some under irradiation in a fission reactor, the closest we have been able to come to testing permeation barriers under fusion reactor-like conditions. Finally, in Section 6, it is considered how design characteristics of permeation experiments may affect the scientific results being generated. Throughout this paper, scientific results will be discussed, grouped by characteristics of the experimental setup with which and the conditions under which these were obtained.

There have been many review papers on permeation barriers focussing on either the substrate or coating materials. However, this is a review paper on the design and operation of permeation experiments: their configuration, setup, operating procedures, and sample characteristics.

2. Theory

The permeation process consists of 6 distinct steps: adsorption, dissociation, absorption, diffusion, recombination, and desorption. In this section, the theoretical description of these different steps, and how the governing quantities are related to each other will be presented.

2.1. Dissolving and recombination

Hydrogen isotopes dissolve in metals in atomic form. Gas molecules adsorb onto the metal surface after which they break up into atoms (dissociation). Then they absorb into the metal. The combined process of dissociation and absorption is called dissolving. After diffusing through the metal, the atoms need to recombine on the other side of the metal before being desorbed in molecular form (Fig. 1), except at extremely high temperatures [1]. Hydrogen can dissolve in molecular form in more open structures.

Considering atomic dissolving, a thermodynamic equilibrium will be reached between the particles in the gas phase in molecular form and dissolved in atomic form, as a result of simultaneous dissolving and recombination:

$$\frac{1}{2}Q_2(g) \leftrightarrow Q(\mathrm{sol}) \tag{1}$$

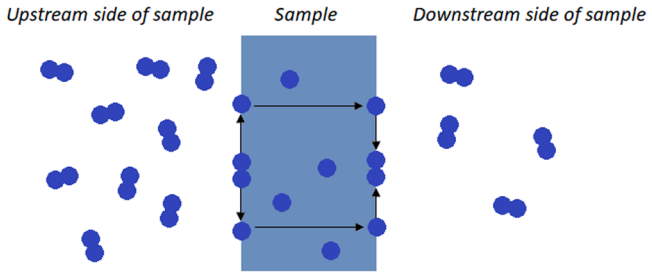

Fig. 1. Simplified diagram of the permeation process.

The equilibrium constant of this reaction obeys Sievert's law and is given by:

$$K_S = \frac{[Q_{sol}]}{[Q_{2(g)}]^{\frac{1}{2}}} = \frac{C_Q}{\sqrt{p_{Q_2}}} \tag{2}$$

Hence K_S has units mol m^{-3} $Pa^{-1/2}$. In the rest of this paper the quantity mol will denote the number of gas molecules Q_2, even though for every mol of gas molecules there will be 2 mol of atoms dissolved in the metal.

The dissociation flux density of atoms into the metal depends on the pressure above the metal and the dissociation constant K_d [10]:

$$J_d = K_d p \tag{3}$$

Here p is the pressure (in Pa) and K_d has units Pa^{-1} m^{-2} s^{-1}. The recombination flux density of atoms out of the metal is proportional to the square of the concentration of hydrogen atoms at the surface, since two atoms are needed to form a molecule [10]:

$$J_r = K_r C^2 \tag{4}$$

Here C is the concentration of atoms (in mol m^{-3}) and the recombination constant K_r has units of mol^{-2} m^4 s^{-1}. In the absence of a concentration gradient or hyperthermal atoms that may enter the metal, the dissociation flux (2) and recombination flux (3) are in equilibrium with each other. This gives the following relationship:

$$K_r C^2 = K_d p \rightarrow C = \sqrt{\frac{K_d}{K_r}}p$$

Here the quantity $\sqrt{K_d/K_r}$ can be recognised as the solubility constant K_S in (1). Similarly, dissolving of diatomic molecules in a metal lattice is described by:

$$Q_2(g) \leftrightarrow Q(sol)$$

Here the equilibrium constant obeys Henry's law and is given by:

$$K_S = \frac{[Q_{sol}]}{[Q_{2(g)}]} = \frac{C_Q}{p_{Q_2}} \tag{5}$$

Both solubility and recombination are thermal processes and are generally described by an Arrhenius equation. Solubility is given by:

$$K_S = K_0 \exp\left(-\frac{\Delta H_s}{RT}\right) \tag{6}$$

Here K_0 is a pre-exponential constant (in mol m^{-3} $Pa^{-1/2}$), ΔH_S is the enthalpy of solution (in J mol^{-1}), R is the universal gas constant (8.3145 J mol^{-1} K^{-1}) and T is the temperature (in K). This is positive for endothermic reactions [1]. Recombination is expressed as follows:

$$K_r = \frac{K_0}{\sqrt{T}} \exp\left(-\frac{E_K}{RT}\right) \tag{7}$$

Here E_K is the activation energy for recombination (in J mol^{-1}), and K_0 is a constant that is related to the solubility, diffusivity, and surface sticking coefficient [1]. The sticking coefficient works against recombination and desorption and is also described by an Arrhenius-like equation [9]. A high recombination rate leads to rapid release, effectively keeping the hydrogen concentration at the surface of the material close to zero. Conversely, a low recombination rate leads to higher inventory of the hydrogen isotopes.

2.2. Diffusivity

Diffusivity is a measure of how easily a particle moves through the metal lattice, in the direction of lower concentration. The flux density of particles that arises from a concentration gradient, in the absence of a temperature gradient, is given by Fick's first law of diffusion [10]:

$$\boldsymbol{J} = -\boldsymbol{D}\,\nabla \boldsymbol{C} \tag{8}$$

with J the flux density (in $m^{-2}\,s^{-1}$), D the diffusivity (in $m^2\,s^{-1}$) and ∇C the concentration gradient (in m^{-4}).

If there is a temperature gradient, Eq. (7) is extended adding a diffusion term caused by the heat of transport Q^* coefficient [10]:

$$\boldsymbol{J} = -\boldsymbol{D}\,\nabla \boldsymbol{C} - \frac{\boldsymbol{D}\,\boldsymbol{Q}^*}{\boldsymbol{R}\,\boldsymbol{T}^2}\,\nabla \boldsymbol{T} \tag{9}$$

In most cases it is assumed that this temperature gradient is negligible, as the thermal conductivity of metals is generally large.

Similar to solubility (5), diffusivity is described by an Arrhenius equation

$$D = D_0 \exp\left(-\frac{E_D}{RT}\right) \tag{10}$$

In this equation, D_0 is a pre-exponential constant (in $m^2\,s^{-1}$) and E_D is the activation energy for diffusion (in J mol^{-1}), R is the gas constant (8.3145 J mol^{-1} K^{-1}) and T the temperature (in K). Both D_0 and E_D are material properties that depend on the diffusing particle. Although (9) describes how the diffusivity depends on temperature, deviations from this relationship are possible due to other effects, especially trapping [1]. See also Section 2.5.

2.3. Isotope effects

Classical theory predicts that the vibrational frequencies and velocities of the different hydrogen isotopes are inversely proportional to $\sqrt{m}$, the square root of their atomic mass. Heavier isotopes will move slower and vibrate at lower frequencies than lighter ones. This implies that the diffusivity also scales with $1/\sqrt{m}$, since the heavier isotope will perform less successful jumps between lattice sites. As a result, the diffusivity of deuterium and tritium are smaller than and can be extrapolated from the values for protium. The activation energy is generally assumed to be independent of the mass of the isotope. This is confirmed in [11], where an isotopic effect in the diffusivity was observed to be very close to $\sqrt{2}$ between hydrogen and deuterium. In contrast, it is assumed that the solubility is the same for all hydrogen isotopes.

However, [12] predicts, using the quantum harmonic approximation for vibrations of atoms in a lattice, that the magnitude of isotope effects depends on temperature. In [10,13] the isotopic effects on the activation energy for diffusion are investigated, with the main conclusion that all metals can demonstrate both a normal isotope effect and an inverted isotope effect. This is because the activation levels for the different hydrogen isotopes decrease with temperature at different rates. As a result, at low temperatures the activation energy for protium is lower than for deuterium and tritium, while at higher temperature this order gets inverted. The temperature at which this transition occurs seems to depend on the lattice structure of the metals; a wide study [14] into the isotope effect of hydrogen and deuterium diffusion through materials concluded that BCC metals demonstrate a normal isotope effect while FCC metals demonstrate an inverted isotope effect at the temperatures studied.

A transient behaviour where the isotope effect depends on temperature was found in [15] by studying a RAFM steel with titanium replacing tantalum. Permeation characteristics were determined for H and D experimentally, with results for T obtained by simulation. Isotope effects for solubility between H, D and T were observed between 1: 1.19: 1.44 at 600 °C to 1: 1.34: 1.53 at 160 °C. This is smaller than the predicted value from $\sqrt{m}$ of 1: $\sqrt{2}$: $\sqrt{3}$ = 1: 1.41: 1.73. The ratio between solubilities, which is expected to show no isotope effect, increased from 1: 1.25: 1.37 at 600 °C to 1: 1.42: 1.72 at 160 °C, clearly showing a relationship with isotope mass and temperature. These results fit the quantum harmonic approximation that is derived in [12].

Permeation fluxes of D and T after implantation in W were studied in [16], where it was found that the steady-state fluxes were nearly constant and independent of the temperature, but proportional to the incident ion energy. However, an isotope effect was observed for the transient behaviour (the time delay); it was found that tritium had a larger activation energy of diffusion than deuterium. The authors stated this agrees with the theoretical isotope effect expected for BCC materials; an increase in activation energy with the mass, reducing the diffusion rate.

Moreover, the PRF of a coating can be different depending on which isotope is permeating. Testing Al_2O_3/FeAl coatings on steel, a comparable, although slightly lower PRF for tritium compared to deuterium was found below 600 °C, while the PRF was 2–3x higher for tritium than for deuterium between 600 and 700 °C [17]. No explanation for this large discrepancy was given.

Questions also arise on whether the radioactivity of tritium influences its diffusivity, solubility, and permeability. However, the factors described above make it difficult to distinguish different isotope effects from each other, making it impossible to answer these questions with data currently available.

2.4. Diffusion-limited and surface-limited regimes

When discussing the effect of pressure on the rate of hydrogen transport through metals, there are two regimes that can be distinguished: the diffusion-limited regime and the surface-limited regime. This depends on the pressure gradient across the boundary.

Imagine that a gas is instantaneously introduced on the upstream side of a metal. This upstream pressure p_1 induces a concentration C_1 on the upstream side according to (1), while the concentration on the downstream side is zero. This creates a concentration gradient through the metal, giving rise to a diffusion flux as described in (7). In this scenario, the flux of particles through the metal depends on the diffusion rate, and this is called the diffusion-limited regime; there is a large pressure difference between the up- and downstream side. The flux density of particles through the metal is in this case given by combining Eqs. (7) and (1), where $\nabla C = C_1/d$, the upstream concentration divided by the thickness d (in m) of the metal:

$$J = \frac{DK_S}{d}\left(\sqrt{p_1}\right) \tag{11}$$

This formula gives the flux density of particles per unit area (m^{-2}). The total flux can be found by multiplying this with the surface area S that is in contact with the gas. The subscript of p_1 can be dropped as the pressure on the downstream side is zero. This gives the permeation flux for the diffusion-limited regime (DLR):

$$\mathscr{J} = S\frac{DK_S}{d}\sqrt{p} \tag{12}$$

The permeability P (in units mol m^{-1} s^{-1} $Pa^{-1/2}$) of a metal is defined as the product DK_S, and as such can also be expressed by an Arrhenius equation:

$$P = D_0 K_0 \exp\left(-\frac{E_D + \Delta H_S}{RT}\right) = P_0 \exp\left(-\frac{E_P}{RT}\right) \tag{13}$$

However, if the concentration gradient through the metal is very small or zero, the rate of permeation is determined by the processes happening at the surface. In this case the permeation flux density, given by the recombination flux density (3) on the downstream side, equals the dissociation flux density (2) on the upstream side minus the recombination on the upstream side:

$$J = K_d p - \frac{1}{2}K_r C^2$$

The factor $\frac{1}{2}$ is introduced as only one side of the metal is considered. Using the relationship $\sqrt{K_d/K_r} = K_S$ found earlier, this equation can be simplified to give the permeation flux density in the surface-limited

regime (SLR):

$$J = \frac{1}{2} K_d p$$

Note here that this is again a flux density, with the total flux given by:

$$\mathscr{J} = \frac{1}{2}\, SK_d p \tag{14}$$

This shows that in the surface-limited regime the flux depends linearly on the pressure, following Henry's law, even though diffusion may take place in atomic form.

Equating (11) and (13) gives the transition pressure between the two regimes: $p = \left(\frac{2DK_S}{dK_d}\right)^2$. The two regimes are not clear-cut as impurities on the surface, such as moisture or the presence of oxygen, can change the kinetic mechanisms and the balance between surface-limited and diffusion-limited processes. The rate-determining process can be determined from the mathematical dependence of the permeability on the pressure, derived from experimental results.

2.5. Trapping

Defects in the metal lattice, such as vacancies, dislocations and grain boundaries can act as trapping sites for the diffusing atom, which reduces the effective diffusion rate. The concentration of trapping sites is generally increased by radiation damage but can also be reduced by recrystallisation processes. Although trapping may reduce the permeation rates, it poses a different challenge by increasing the amount of hydrogen isotopes (especially tritium) lost and retained in the materials.

Trapping is a thermal process; the trapped atom needs to overcome an energy barrier to leave the trap and start diffusing again. This energy is generally larger than the activation energy for diffusion. The effective diffusivity[1] is calculated from the diffusivity by

$$D_{eff} = \frac{D}{1 + \frac{C_T}{C_L} \exp\left(\frac{E_T - E_S}{RT}\right)}$$

Where C_T is the concentration of trapping sites (in mol m^{-3}), C_L the concentration of lattice sites (in mol m^{-3}), E_T the trapping energy and E_S is the enthalpy of solution (both in J mol^{-1}) into interstitial sites. This relationship indicates that D_{eff} is lower than D at lower temperatures, but similar when the temperature is increased, thus trapping effects can be ignored at elevated temperatures. When studying the relationship between effective diffusivity and temperature, this breaking point has been observed around 250 °C, causing a clear change in gradient in the graphs of D_{eff} as function of $1/T$ [1].

2.6. Plasma-driven permeation

The equations derived earlier all depend on the pressure of a gas above the metal. However, plasma-facing components in future fusion reactors will be exposed to ions in a hot deuterium-tritium plasma, which are able to migrate into the materials due to their abundant energy. Due to their high energy, they can be deposited at some depth in the material, this is called the implantation zone. Once implanted, these atoms can diffuse and permeate through the metal, similar to atoms that have entered the metal from the gas phase. This gives rise to plasma-driven permeation (PDP), as opposed to gas-driven permeation (GDP).

Instead of two regimes (diffusion-limited and surface-limited) there are now three different regimes due to the distinctive difference between the plasma facing side and the permeate side [1]:

- DD (diffusion limited both upstream and downstream); hydrogen is deeply implanted, and diffusion is slow compared to recombination. The concentration is highest at the maximum implantation depth, decreasing in both directions due to the recombination taking place on both surfaces.
- RD (recombination limited upstream and diffusion limited downstream); hydrogen concentration is relatively constant throughout the implantation zone where recombination is limited. The concentration drops off deeper inside the metal and towards the permeate side.
- RR (recombination limited both upstream and downstream); the hydrogen concentration is uniform throughout.

This paper will focus on gas-driven permeation only. It is recommended that a similar review will be conducted for plasma-driven permeation.

2.7. Anti-permeation coatings

To reduce the permeation of tritium through structural metals used in a fusion reactor, a coating with a lower permeability can be applied to this metal. The effectiveness of the coating can be determined by measuring the permeation rate through the bare substrate and through the substrate with coating, under identical pressure and temperature conditions. This gives the PRF [1]:

$$PRF = \frac{\mathscr{J}_{uncoated}}{\mathscr{J}_{coated}} \tag{15}$$

A coating system performs better if it has a higher PRF. Coatings have been developed with a PRF as high as 10^3 – 10^4 [17–21].

2.7.1. Factors influencing the PRF

The PRF will not necessarily change proportionally to the thickness of the coating, as there are many other factors at play, such as the number of layers, the deposition method, the conditions of the coating such as defect density, and the side of the metal that is coated. These factors are discussed in Section 3.3. It is important to note here that these factors only hold for the combination of substrate and coating, not for coatings separately. Furthermore, thin films have a different structure and grain size from bulk material, which makes it difficult to predict the performance of a material as permeation barrier from its bulk properties. In general, results obtained using ceramic bulk materials suggest a better permeation reduction performance than experimentally demonstrated using coatings of this material, possibly due to defects in the coating [2].

There are many unknowns in predicting permeation through a composite of layers, and there are different models that describe this process [4]. These are:

- Composite Diffusion Model
  Hydrogen transport is diffusion-controlled in both the coating and the substrate. Permeation is simply controlled by the permeation through the coating, which has a lower permeability than the bulk material.
- Area Defect Model
  The permeation barrier is effectively impermeable. Hydrogen diffuses through the bulk material, reaching the surface through a limited number of cracks or other defects in the barrier layer. Permeation effectively takes place through a reduced surface area.
- Surface Desorption Model
  Permeation is controlled by the recombination rate of hydrogen isotope atoms into molecules on the back surface. In this context, it is difficult to visualise what effect a coating on the upstream side has on the permeation rate.

Analysis of permeation rates, through coated and uncoated

[1] Assuming that there is only one detrapping energy and that all traps can only be occupied by a single atomic species.

materials, is needed to determine which model is most appropriate to describe permeation through a layered material. It is important to note here that both the Composite Diffusion Model and Area Defect Model suggest that the permeation process is diffusion-limited, hence should depend on the square root of the pressure (Sievert's law), while the Surface Desorption Model assumes a linear dependence (Henry's law) [4]. Further, different techniques for coating application could be studied to determine whether the Area Defect Model can be dismissed.

There are also other processes that can act as a permeation barrier. For example, magnetohydrodynamic effects lead to a velocity profile in the LiPb eutectic with slow moving tritium at the boundaries. This creates an effective boundary layer between the liquid metal and the coolant walls. In this boundary layer, tritium transport occurs through convection. This creates a resistance effect that has been estimated to be equivalent to a PRF between 30 and 50 [6].

2.8. Measurements of transport coefficients

The most intuitive and commonly used way of determining the permeation rate through a sample is by determining the steady-state permeation flux, given by (11). *A sample of the material in question with a specific surface area S and thickness d is placed in a chamber, dividing this into an upstream and downstream section. It is exposed on the upstream side to a process gas of known pressure p at constant temperature T, with no process gas present on the downstream side to ensure the diffusion-limited regime. The increase in pressure due to permeation is monitored, and the permeability P can be determined from the steady-state permeation flux. This is sometimes called the continuous flow method [15,22] or pressure-rise method [23]. The diffusivity D can be determined from the time-dependence of the permeation flux, explained below, after which the solubility can be found using* $K_S = P/D$.

An expression for the permeation flux density as function of time can be derived starting with Fick's first law of diffusion (7). *Imposing conservation of the number of particles gives Fick's second law of diffusion:*

$$\frac{\partial C}{\partial t} = -\nabla J = D\,\nabla^2 C \tag{16}$$

In case of a one-dimensional membrane, the substitution $\nabla^2 \rightarrow \frac{\partial^2}{\partial x^2}$ *can be made, with the upstream side of the membrane positioned at* $x = 0$ *and the downstream side at* $x = d$. *A solution for* $C(t,x)$ *can be found by matching the boundary conditions* $C(t=0,x)=0$, $C(t>0,\ x=0)=C_0$ *and* $C(t>0,x=d)=0$ [10]:

$$C(t,x) = C_0\left(1-\frac{x}{d}\right) - C_0 \times \left[\frac{2}{\pi}\sum_{n=1}\frac{1}{n}\sin\left(\frac{n\pi}{d}x\right)\exp\left(-\frac{Dn^2\pi^2}{d^2}t\right)\right]$$

From this expression of C(t, x) *the diffusive flux density can be found:*

$$J(t) = -D\frac{\partial C}{\partial x} = \frac{DC_0}{d} + \frac{2DC_0}{d}\left[\sum_n \cos\left(\frac{n\pi}{d}x\right)\exp\left(-\frac{Dn^2\pi^2}{d^2}t\right)\right]$$

The diffusive flux density leaving the membrane (i.e., *permeating through) is found by setting* $x = d$:

$$J(t) = -D\frac{\partial C}{\partial x} = \frac{DC_0}{d} + \frac{2DC_0}{d}\left[\sum_n (-1)^n \exp\left(-\frac{Dn^2\pi^2}{d^2}t\right)\right] \tag{17}$$

From (16) *the flux density found in* (12) *can be found, using the relationship between solubility and concentration* (1), *multiplying by the surface area S and taking the limit* $t \rightarrow \infty$.

The total amount permeated per unit surface area can be found by integrating (16) *with respect to time:*

$$\Phi(t) = \int_0^t J(t')dt'$$
$$= \frac{DC_0}{d}t + \frac{2dC_0}{\pi^2}\sum_n \frac{(-1)^n}{n^2} - \frac{2dC_0}{\pi^2}\sum_n \frac{(-1)^n}{n^2}\exp\left(-\frac{Dn^2\pi^2}{d^2}t\right)$$

The sum in the second and third terms is a standard infinite sum.[2] *Inserting* (1) *simplifies* $\Phi(t)$ *to:*

$$\Phi(t) = \frac{DK_S\sqrt{p}}{d}t - \frac{dK_S\sqrt{p}}{6} + \frac{2dK_S\sqrt{p}}{\pi^2}\sum_n \frac{(-1)^n}{n^2}\exp\left(-\frac{Dn^2\pi^2}{d^2}t\right) \tag{18}$$

In the steady-state limit $t \rightarrow \infty$, this reduces to

$$\Phi(t) = \frac{DK_S\sqrt{p}}{d}t - \frac{dK_S\sqrt{p}}{6} \tag{19}$$

A schematic graph showing an approximation to (17) and (18) is shown in Fig. 2. Eq. (18) describes a linear graph with an intersection of the t-axis at [1,10]:

$$t = \frac{d^2}{6D} \tag{20}$$

This is called the time-lag method, where the time $t = 0$ is the moment that gas is introduced on the upstream side. Alternatively, the breakthrough method can be adopted which defines $t = 0$ as the moment hydrogen appears on the downstream side. In this case $t = d^2/(15.3D)$ [24].

The amount of permeate $\Phi(t)$ in the downstream section of the sample chamber can be monitored by measuring the pressure in this chamber. Alternatively, when the permeate flux density $J(t)$ is determined by continuously pumping the downstream section, this can be integrated to give $\Phi(t)$.

Adding a coating to a sample will not only change its permeability; it will also change the time for steady-state permeation to be established, and hence the resultant diffusivity of the coating and substrate together [1]. In this case, the resultant diffusivity D_{res} is found by using the time-lag method [23]:

$$D_{res} = \left(\frac{d_s + d_c}{6t}\right)$$

By performing the same experiment at different pressures and determining the permeation flux, the pressure exponent can be determined. A change in the exponent with changing temperature has been reported for a Y_2O_3 *coating on 316* L *stainless steel [25]; the exponent was observed to change from 0.47 at 500* °C *to 0.74 at 650* °C. *This indicates a transition from the DLR to SLR.*

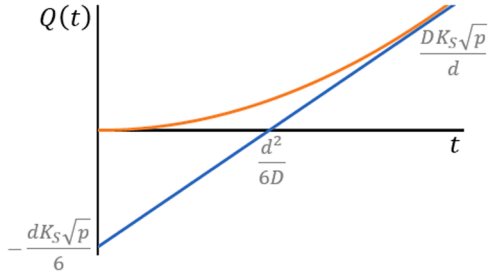

Fig. 2. Graph showing the relationship between the amount permeated per unit surface area as described by Eq. (18) and the time delay as defined in Eq. (19). The actual amount permeated (17) is shown in orange, the approximation for steady-state permeation (18) in blue.

[2] $\sum_n \frac{(-1)^n}{n^2} = -\frac{\pi^2}{12}$.

However, a composite coating of Y_2O_3 and Al_2O_3 proved to have a very stable exponent with changing temperature.

Practical implications of performing permeation experiments will be followed up in Section 6.

3. Materials

The research into materials for tritium permeation barriers is an extensive field of study, with several possible coatings to be applied to various candidates for structural materials, using numerous different deposition techniques. This leads to a large number of potential hydrogen permeation barrier candidates.

These candidates are subject to various experiments, testing not only their performance under varying conditions, but also their durability under repeated heating cycles, their resistance to hydrogen embrittlement and blistering, the attachment of the coating to the substrate, and the effects of exposure to corrosive substances such as LiPb, used in several tritium breeding concepts.

Additionally, these materials must operate in a challenging radiation environment. The radiation dose of the breeder blanket materials can be estimated at a neutron fluence of 10^{21} n/m^2 [26] with a total displacement of 1.2 dpa after 6 FPY (full power years). In addition to neutron radiation, there will also be gamma radiation present. The coatings that are needed to reduce tritium permeation, might fail in radiation environments [9] as radiation increases the porosity or cracks in the barrier.

There have been various review papers published discussing tritium permeation barrier materials, for example [1,2,4,10,27–30]. As such, the main candidates will be discussed here very briefly only to give context for the reader.

3.1. Structural materials

The main candidates for structural material include tungsten, austenitic stainless steels, RAFM steels and some nickel-based alloys [1, 10,30].

3.1.1. Tungsten

Tungsten (W) is being used in many fusion reactors due to its high melting point and low sputtering yield, making it an ideal candidate for Plasma Facing Components (PFCs) [10]. Diffusion through tungsten is a complex process with defects, trapping and implantation of hydrogen influencing the diffusion rate considerably [28]. Hydrogen retained in tungsten is trapped in saturated layers, which can grow in thickness far over the implanted depth [29]. It is therefore in an uncoated state not a suitable candidate for a tritium permeation barrier.

3.1.2. Austenitic stainless steels

Austenitic stainless steels have been extensively used in fission power plants. Unfortunately, they contain Ni acting as stabilizer which makes them unfavourable to use in a fusion power plant due to the high susceptibility of Ni to activation [9]. The permeability of austenitic stainless steels is generally lower than other structural materials, especially at low temperatures, and seems independent of alloy composition [10]. This can generally be attributed to the low diffusivity, however, the activation energy for diffusion is relatively large, making diffusivity sensitive to temperature. In contrast, the solubility of hydrogen and its isotopes is large in austenitic stainless steels compared to other structural steels and the heat of dissolution is significantly lower than in other metals [9]. As a result, the tritium inventory in austenitic stainless steels can be relatively high even at low temperatures. Examples of commonly used austenitic stainless steels are 304, 316 and 316 L stainless steel.

3.1.3. RAFM steels

Several reduced activation ferritic/martensitic (RAFM) steels have been developed for fusion applications, due to their reduced activation under neutron irradiation. This is achieved by replacing alloying elements such as Mo and Nb by W and Ta and restricting other elements (such as Ni, Co, Cu, Nb, Mo, Ag) highly in their concentrations [9]. RAFM steels also demonstrate an increased swelling resistance and are compatible with breeding and cooling materials [10]. Examples of RAFM steels are MANET (MArtensitic for NET, including the so-called MANET II) and modified F82H (generally referred to as F82H- mod), EUROFER 97, Batman, OPTIFER-IVb, HT-9, grade 91, JLF-1 and CLAM steel [9].

The diffusivities and solubilities of hydrogen isotopes are consistently similar for all the RAFM steels that have been tested for fusion applications [9]. Trapping affects the diffusivity and solubility significantly, reducing the diffusivity and increasing the solubility at lower temperatures (< 573 K) to a larger extent than expected from tests at higher temperatures [10]. These trapping effects can be ignored at higher temperatures as the hydrogen isotopes will have energies that exceed the de-trapping energy. Further, the solubility is governed by the heat of solution, hence there is no isotopic effect [1]. The permeability of RAFM steels is of the same order of magnitude and generally higher than 316 stainless steel due to different crystal structures and alloying elements [1]. RAFM steels face disadvantages in fusion applications because of their low temperature embrittlement and their tendency to retain hydrogen due to the formation of saturated surface layers [1].

3.1.4. Nickel-based alloys

Nickel based alloys are prime candidates for high-temperature components due to their resistance to high-temperature creep. Examples are Inconel 625, Inconel 617 and Incoloy 800H The latter two have been tested in [31], finding a substantial deviation in results obtained with tritium compared to hydrogen. Unfortunately, no explanation was given. Inconel-625 and Inconel-718 have been studied in [32]. However, nickel-based alloys have seen less interest than iron-based alloys.

3.2. Coating materials

As explained in the previous section, structural metals by themselves are not good permeation barriers, having high hydrogen permeabilities. Applying a coating can reduce the permeability and additionally provide corrosion resistance and irradiation shielding. This is especially important for liquid breeder blankets, as liquid lithium can cause embrittlement [2]. Furthermore, ceramic permeation barriers are electrical insulators and can help to mitigate magnetohydrodynamic pressure drops.

The available data on permeation reduction by coatings vary greatly due to differences in quality of the coating (such as surface coverage, defect density and crystallinity), possibly a result of the application process and the variety of substrates. The application process alone can have a significant effect on the permeation reducing performance of the coating, sometimes 10-fold [28]. Further factors complicating the assessment are the coating thicknesses, test temperatures, other process variables and experimental conditions used by different researchers. The most common coating materials are discussed below.

3.2.1. Oxides

Oxide layers form naturally on the surface of metals when oxygen is present. They generally have very low permeabilities for hydrogen isotopes, and native oxide layers may reduce the permeability by about an order of magnitude [28]. Attractive properties of oxide layers are the ability to form on uneven surfaces, although this depends on the surface roughness, and the capacity to self-heal when damaged or even grow under the right circumstances. However, the coefficient for thermal expansion is often quite different from the underlying metal. Oxide layers also provide trapping sites for hydrogen, leading to a more brittle layer and an increased tritium inventory. These effects can cause the formation of cracks, which reduces the effectiveness of the barrier [9].

As early as in 1996 it was observed that adding oxygen to the

downstream side of an uncoated sample reduced the permeation rate below 423 K, suggesting an oxide layer had formed [33]. Common examples of oxides that have been tested as hydrogen permeation barriers are chromium oxide, aluminium oxide, erbium oxide and yttrium oxide. Aluminium oxide deposited on Eurofer has been shown to have a PRF of ~1000 [34]. In other tests aluminium oxide was shown to provide a PRF of 10^4 with layers of only very small thicknesses [4]. Mixtures of chromium oxide and aluminium oxide also perform very well with a PRF of 2000–3500 [35]. While erbium oxide and yttrium oxide may not excel in their permeation reduction performance, they have the advantage of being compatible with liquid lithium [9]. However, even these coatings are subject to degradation over time.

3.2.2. Aluminides

The use of aluminides as anti-permeation coatings arose from previous work undertaken on oxide coatings, as explained in [4]. Aluminium coatings can oxidise even at very low oxygen pressures, reducing the hydrogen permeation even further.

Intermetallic layers such as Fe_xAl_y can be formed using cementation techniques, forming an outer layer with the highest aluminium concentration and a decreasing aluminium gradient in the inner layer [4]. However, no permeation tests have been performed on oxide-free aluminium coatings [9].

3.2.3. Nitrides

Several nitrides have been tested for their permeation reduction performance. Titanium nitrides (TiN) coatings are one of the most researched barriers after oxides and aluminide, for their depositions and adhesion performance [9].

When deposited using a magnetically enhanced plasma ion plating technique a TiN coating demonstrated a PRF ~100 but when deposited using magnetron sputtering this PRF was ~1100. Adding aluminium improves the resistance of TiN coatings to an oxidative atmosphere. PRF values of between 6×10^3 and 2×10^4 were observed for AlTiN with a ratio of Al:Ti of 40:60, but in some cases this performance did not last longer than a few days [28].

Silicon nitrides (SiN) have been tested and show a very low diffusivity, but a PRF of 2000 has only been determined at very specific circumstances [28].

3.2.4. Carbides

Carbides could theoretically perform well as permeation barrier. However, it has proved to be extremely difficult to form a dense and defect-free coating. Titanium carbide (TiC) has turned out to be very difficult to deposit, demonstrating a low PRF due to defects in the coating [9]. Silicon carbide (SiC) has been tested as permeation barrier at 1873 K. Extrapolating these results suggests a very low PRF at lower temperatures, but this has yet to be verified [28].

3.3. Coating characteristics

As briefly mentioned in the previous section, identical coating materials can perform differently depending on the deposition method used. These methods can be classified in four categories: thermal spray, physical vapour, chemical and electrochemical deposition processes. Each method has its own advantages and disadvantages, for example whether the coating can be applied on complex geometries or which coating material can be deposited. The coating method can affect the microstructure and defect density of the coating, influencing the permeation process.

In [1] two different coating methods, Vacuum Plasma Spray (VPS) and sputter deposited (SP), of tungsten on F82H were investigated for their reduction of both PDP and GDP. It was found that the VPS layers suppress PDP, but not GDP, while the SP layers suppress GDP but enhance PDP. However, a double layer of both VPS/SP can suppress both GDP and PDP [1]. A further study [36] investigated yttrium oxide coatings with different grain sizes and orientations on Eurofer, and found that the density of grain boundaries in the parallel direction to the flux determines the PRF; a higher density of grain boundaries leads to a lower PRF. This is an important effect as irradiation of the coating can change the grain size; how the evolution of such coating characteristics under irradiation and contamination affects permeation rates will be discussed in Sections 4.7 and 4.8.

A coating's surface coverage of the sample also influences its performance. Several studies have tried to model the effect of uncovered areas on the PRF. It was estimated that the effectiveness of an erbium oxide coating with a PRF of 1000 would be reduced to a PRF of 100 if 1 % of the surface remained uncovered [2]. However, it was shown in [37] that the effect of reduction of surface coverage on the PRF depends on the permeation regime; if the permeation is diffusion-limited a small uncovered fraction of the surface (0.01 %) could effectively lead to having no coating at all (PRF=1). To obtain a similar reduction in the surface-limited regime, the area uncovered must be close to 100 % of the surface. However, when a coating is applied to also serve as corrosion or electrically insulating barrier, a very high surface coverage is required independent of the permeation process.

Other characteristics that determine how effective a coating is in reducing permeation include the thickness of the coating, whether the coating is applied on the upstream or downstream side of the sample (or both), and the number of layers applied.

When testing the reduction performance of coatings with different thicknesses [38], it was found that the thickness relates inversely to the reduction performance; a coating of 1.3 μm corresponded to a 2x higher flux than a coating of 2.6 μm thickness. However, this assumed that there were no cracks in the coating that reached the substrate, as deep cracks will increase the permeation rate. The PRF does not necessarily increase inversely with coating thickness; the authors of [39] tested two different ZrO_2 coatings; a 180 nm coating and a 100 nm coating. The thicker coating had a 1000 times higher permeation reduction factor, even though it was not yet twice as thick. The authors attributed this to a smaller number of defects reaching the substrate surface.

In another study [40] it was found that applying two thin layers of coating, one on either side of the sample, performed better than a one-sided coating of the same total thickness. Further, the same study found that applying a coating on the downstream side of the sample was less effective in reducing the permeation than a coating on the upstream side, probably due to the different partial pressures and contamination levels.

These findings are supported by experiments conducted on TiN barriers deposited on stainless steel, where it was found that these coatings reduced permeability the most when they were placed on the upstream side of samples, and a much smaller change in permeation was observed when they were placed on the downstream side [40,41].

The effect of applying a single Er_2O_3 coating, a two-layer coating of Er_2O_3 and Fe, or three-layer coating of alternating Er_2O_3 and Fe layers on a Fe substrate was investigated in [42]. The two-layer coating performed similarly to the single layer coating, demonstrating a PRF of 1000, while the 3-layer coating reduced the permeation by a factor 10^4. This is probably due to the presence of two layers of Er_2O_3 and the increased thickness. Depth-analysis showed that the amount of deuterium trapped in the 3-layer coating was 3 times higher than in the 2-layer coating.

Further, evidence has been provided that increasing the number of layers while keeping the total thickness constant can also be beneficial [25]. Multi-layer coatings made up of 10 layers were tested, each consisting of 20 nm layers of Y_2O_3 and 10 nm layers of Al_2O_3. Compared to their single-layer counterparts with the same thickness, these coatings reduced the permeation rate 5–10 times. This can be explained by possible trapping at the interfaces between the layers.

Moreover, depending on the coating material and the substances it gets exposed to, the coating can be degraded (for example by the action of LiPb) or, in the case of oxides, self-heal when brought in contact with

oxygen. These effects are discussed in Section 4.8.

Finally, it is important to realise that a multi-layer tritium permeation barrier may be effective at reducing permeation but will increase the tritium inventory trapped in the system. This is not desirable for future fusion power plants as it will lead to high tritium losses and high contamination levels during decommissioning. It is not known whether a large amount of tritium trapped in the layers will lead to an increase in the permeation rate when it reaches a critical concentration. No experiments have been performed that investigated the possibility of such a breakthrough event. If this were the case, such coatings could only be used in fusion power plants for a limited amount of time; they would have to be replaced frequently when their performance diminishes, and large amounts of tritium would have to be recovered from them. It is therefore preferred to find a coating that performs well without trapping too much tritium, e.g. a coating applied on the upstream side of the material, keeping the tritium out of the bulk.

4. Experimental limitations

There have been numerous experiments studying hydrogen permeation through materials, agreeing partially with the theory as explained in Section 2 but also giving unexpected results, such as different PRFs obtained for different isotopes [17], or the effect that the deposition method has on reducing PDP and GDP [1]. These results are proof that theory cannot always predict experimental outcomes precisely, and that ideal conditions cannot be realised experimentally. However, there may be an even larger discrepancy between what theory predicts and what will occur in fusion reactors, as scientific experiments are limited in the conditions that can be simulated and there is still a wide gap between experimental conditions and fusion reactor conditions.

In this section, different factors affecting the permeation rate will be discussed, highlighting the limitations of current experiments and efforts to cross the gap between experiment and (future) reality. These factors include pressure, temperature, flow rate, the presence of other hydrogen isotopes, geometry, irradiation effects, and contamination of the coating.

4.1. Pressure

As explained in Section 2.4, when increasing the pressure a transition occurs from surface-limited to diffusion-limited permeation. Of the 43 papers studying permeation through structural materials such as stainless steels, Eurofer, F82H and tungsten that were considered for this review paper, 27 used a driving pressure of 10^3 – 10^5 Pa to obtain a measurable permeation flux [15,17,21,23–25,34,36,38–40,42–56], with the remaining 16 operating at pressures of the order of 10^2 Pa or lower. Typical tritium pressures in breeder blankets are expected to be around 200 Pa [57], which is assumed to be in the SLR [28]. It is unlikely that all results obtained in experiments performed at higher pressures can be extrapolated to lower pressures as surface mechanisms play a more important role in this regime. As a result, surface effects may go unnoticed in some experiments, highlighting the need for experimental methods that can study tritium permeation in the surface-limited regime.

4.2. Temperature

The temperature dependence of both diffusion and dissolving rates are given by their respective formulas, (9) and (5), both describing an Arrhenius dependence. It can generally be assumed that there is no temperature gradient under experimental conditions due to the high thermal conductivity of the structural materials. However, it is likely that cooling located in breeder blankets will cause a temperature gradient across the material.

The effect of a temperature gradient on deuterium permeation has been tested on 316 L stainless steel [58]. It was found that deuterium permeation was increased by a factor ~2.5 under a temperature gradient of ~ 60 °C/mm, with the sample being heated to temperatures between 270 °C and 400 °C on one side. This highlights the need to study this effect further, as cooling seems to enhance the permeation, contrary to what may be expected from the theoretical dependency of permeation on temperature.

Further, anti-permeation coatings might perform worse at certain (higher) temperatures due to degradation, hence they will need to be tested at these temperatures. In addition, trapping effects can affect the effective diffusivity to varying degrees at different temperatures, as mentioned in Section 2.5. As such, it is not recommended to extrapolate from the results on coating performance obtained at one temperature to other temperatures.

4.3. Flowing gases

The theory of permeation (12) does not include a reference to the flow rate of gases, either on the upstream or downstream side of the barrier. However, it is likely there are dynamic effects that influence the rate at which gases absorb onto and desorb from a surface.

Simulations on a tritium breeding module [59] have shown that the purge gas flow rate on the upstream side plays an important role in reducing the tritium permeation, displaying an almost linear relationship between permeation rate and average velocity. Another numerical model on solid breeder blankets [60] found that when the flow rate of the purge gas, aimed at extracting tritium from the breeder, is increased, the concentration of tritium in this gas decreases by the same magnitude, also reducing the permeation into the coolant.

The majority of permeation experiments have been performed in a “static” setup; two vacuum chambers separated by the sample. The permeation rate can be determined by measuring the increase in pressure on the downstream side or analysing the gas with a mass spectrometer. There have only been a few experiments that have used flowing gases: either using flowing gases on both sides [33,61–63] or only on one side [17]. These experimental conditions are more similar to future applications in fusion reactors than static vacuum configurations and may generate results that could deviate significantly from those obtained in a static configuration.

However, in these studies the velocity of the gases has not been the topic of investigation, nor have there been attempts to compare results obtained with flowing gases to results from static experiments. It has been shown that the flow rate does influence the absorption rate in absorption columns for purifying gases [64], suggesting that this may also have an effect on the inverse process, i.e. desorption. Further, numerical models [59,60] suggest that the gas velocity does affect the permeation rate. Hence it would be worthwhile validating permeation models with results from both static and dynamic experiments.

4.4. Gas composition and the presence of more than one hydrogen isotope

The theory of permeation (see Section 2) states that, when considering the permeation of one species of gas, the presence of other gases does not affect the permeation rate. Rather, it is the pressure difference between the up- and downstream of the sample that is driving the permeation process. The one exception to this is the possible chemical reduction of oxides on the metal surface by hydrogen which will decrease the average thickness or area coverage of the oxides [65]. This will increase the permeation rate since oxides act as permeation barriers.

The question now arises whether the species into which the hydrogen isotopes permeate, on the downstream side, influences the permeation rate. There is very limited data available to demonstrate this effect. However, it is known that the diffusion rate of one species of particle in a medium depends on several factors in addition to temperature. These are the molecular weight and cross sections of both species and the pressure of the medium. Larger, heavier molecules will slow down diffusion, with a precise relationship given in [66]. In addition,

diffusion into a gas at a higher pressure will be slower than into a gas at a lower pressure. It can be concluded that the gas species on the downstream side of the sample does affect the diffusion rate. However, it is not known whether it also affects the desorption rate from the sample, and whether this difference in diffusion rate can create a temporary higher pressure in the gas on the downstream side.

Gases such as oxygen and carbon monoxide also affect the permeation rate, investigated in [67]. Individually, both O_2 and CO inhibit hydrogen permeation when located on the upstream side of the sample; by blocking available dissociation sites and, in the case of oxygen, the formation of water. However, when both are present carbon dioxide is formed which reduces the blocking effect of water formation.

Adding a second isotope can change the permeation rate of the first isotope [68]. This effect is present both in the diffusion-limited and surface-limited regime even though the exact workings are different, as mathematically explained in [68]. Intuitively, this situation can be understood as follows.

Compared to the situation when only tritium is present at a set pressure, adding either deuterium or protium to the system leads to competition between the isotopes for the same number of absorption sites on the permeation barrier. As such, the permeation rate of tritium will be lower. Furthermore, any permeated tritium can also permeate back to the upstream side. In this case tritium atoms on the upstream side are more likely to form a molecule and be desorbed from the permeation barrier if other isotopes are present, increasing the permeation in the opposite direction. The net effect of this is a decrease in the permeation rate. Following the same logic, the presence of either protium or deuterium on the downstream side of a permeation barrier will enhance the tritium permeation rate.

There have been several experiments, testing these co- and counter permeation effects. The authors of [69] reported their findings on the co-permeation of H and D. Adding D on the upstream side led to the formation of HD, promoting the back permeation of H. However, it also increased the permeation of D slightly. It was found that effects of co-permeation are independent of whether the gas is in equilibrium (consisting of H_2, HD and D_2) or not (only H_2 and D_2 are present) [33,69].

A numerical model for co-permeation of T and H was developed in [63], stating that the permeation rate of T depends on the square root of the tritium pressure and linearly on the HT pressure. These findings were confirmed experimentally for the diffusion-limited regime and were extended in [62], stating that under high H pressure the permeation of T is described by diffusion-limited behaviour, even when the T pressure is very low.

In an experiment on counter-permeation of H and D through palladium, a low pressure of D was introduced on the downstream side. This increased the permeation of H, promoting the formation of HD molecules on the downstream side [70]. It was noticed that the D permeation decreased with increasing counterflow of H but did not disappear completely. Experiments using nickel yielded comparable results [71].

These results show that, although the effects of co- and counter permeation seem to be well understood, surprising results are possible. To study whether, and under which conditions, adding protium to the helium coolant in a Helium Cooled Pebble Bed blanket could have mitigating or enhancing effects on tritium permeation, a new rig has recently been designed and commissioned [72], to test co- and counter permeation of H and D through Eurofer samples. Performing additional experiments using tritium with H and D is recommended, as there may be isotope effects at play that could influence the co- and counter permeation effects.

4.4.1. Permeation experiments using water

There have been very few permeation experiments using water as medium, which may be due to the additional safety concerns when handling tritiated water. However, water is being considered as coolant in several breeder banket concepts and will be present in the steam generator, where the heat captured by the coolant is used to generate steam driving a turbine.

The prevailing experience from working with tritium suggests that tritium will readily bind to water, preferring this over the gas phase. Intentional permeation into a water coolant could be beneficial for control purposes, but this would ideally be avoided due to the toxicity of tritiated water.

Permeation of deuterium from heavy water through a metal wall into the gas phase was studied in [73]. Iron, nickel and 304 stainless steel were used in this study, all demonstrating a permeability between 10^{-11} – 10^{-12} mol m^{-1} s^{-1} $Pa^{-1/2}$ at 573 K. Adding gold plating on the water side reduced the permeation by 3 orders of magnitude.

Tritium permeation from water to water has been studied through 316 L stainless steel [74] and Inconel 600 [75]. It was found that, when the tritium concentration in the water was converted to a gas pressure, the permeation in the gas phase occurred at a rate 3 orders of magnitude higher than in the water phase. This is probably due to the difference in solution processes between water and gas; in gases this is determined by the partial pressure, while in water this is controlled by the presence of radicals such as T^+ or OT^-.

4.5. Geometry

In Section 2.8 the steady-state approximation for the permeation flux was given in Eq. (18), derived for a planar boundary. In [76] the steady-state diffusion through a hollow cylinder is considered. For a cylinder with inner radius a and outer radius b, the amount diffused out of the cylinder per unit length after a given time t is given by:

$$Q_t = 2\pi \frac{C}{\ln(b/a)}(Dt - L)$$

Here C is the concentration of atoms (in mol m^{-3}), D is the diffusivity (in m^2 s^{-1}), t is the time (in s), L is a constant (in m^2) and Q_t is given in mol m^{-1}. This formula describes a straight line with as intersection with the t-axis the point $t = L/D$. According to [76] this L can be evaluated at

$$L = \frac{a^2 - b^2 + \left(a^2 + b^2\right)\, ln(b/a)}{4\, ln(b/a)}$$

Comparing this with the time delay calculated in (19), this shows that the time delay in cylindrical coordinates is equal to

$$t = \frac{a^2 - b^2 + \left(a^2 + b^2\right)\, ln(b/a)}{4\, D\, ln(b/a)} \tag{21}$$

Comparing Eqs. (19) and (20) can provide insight into the accuracy of approximating a tubular surface with a planar one. For a thickness of $b - a$ equal to 1 mm and setting $D = 1$ the time delay can be calculated as function of outer radius b, as shown in Fig. 3. In the most extreme case, a tube with a 1 mm thick wall and outer wall $b \sim 2$ mm (i.e. a solid cylinder with inner diameter $a \sim 0$), the time delay can be evaluated at $\sim \frac{-3+5\ln(2)}{4\ln(2)} \sim 0.16798$ s. For comparison, Eq. (19) for flat samples with $D = 1$ gives a value of $1/6 \sim 0.16667$ s. This accounts for an error of 0.00780, which is <1 %. For wider tubes, this error will only decrease. As such, when the time delay is used to estimate the required time duration of an experiment, the flat approximation can be used. Only when very precise results are required, this effect may need to be considered.

So far, only a few permeation experiments have been performed on coated tubes [17,20,33,73–75]. The difficulty here lies in applying the coating to the inside of the tube. The authors of [20] formed aluminide layers by a pack cementation process on the inside of 316 L stainless steel tubes with a diameter of 10 mm and 150 mm length. The thickness of the layers varied between 200 and 500 nm and a PRF of 3000 was achieved. This shows that it is possible to apply a tritium barrier coating to the inside of a tube, although there have been more experiments that

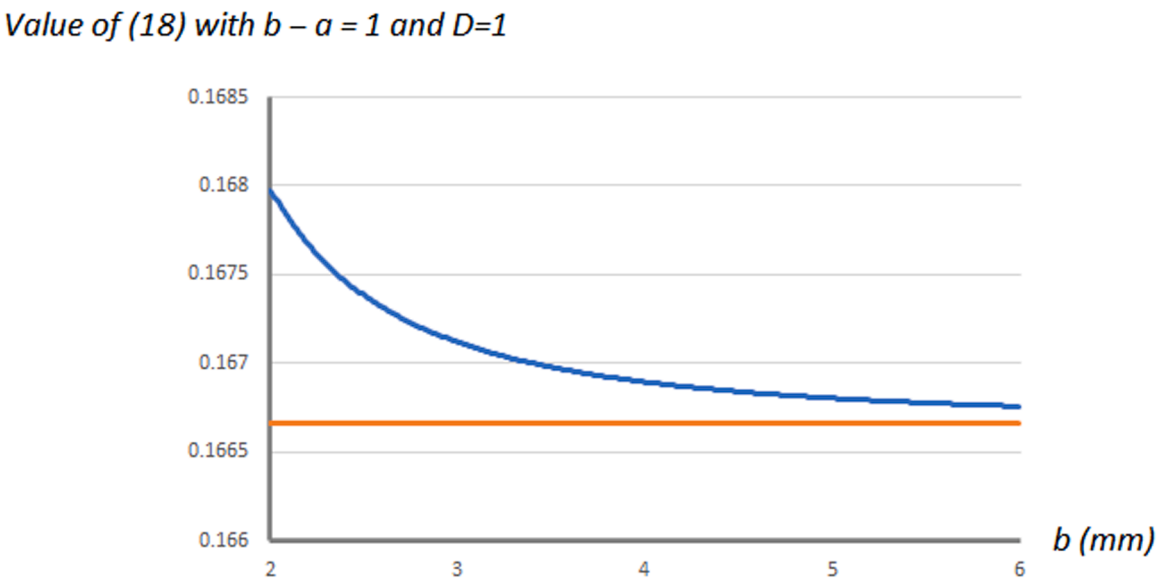

Fig. 3. Time delay for cylinder with thickness (b-a) 1 mm (blue line) as function of outer radius b, assuming $D = 1$. The orange line shows the value 1/6 for flat samples as comparison.

tested coatings on the outside surface. This is potentially an important factor as it has been shown that coatings applied on the upstream side are more effective as permeation barriers than on the downstream side [41]. However, this does not imply that all coatings applied on the downstream side are ineffective; it was shown in [17] that coatings applied on the outside of a stainless-steel tube could obtain a PRF of 5000.

4.6. Gas driven or plasma driven permeation

There have been a few studies into plasma-driven, as opposed to gas-driven, permeation. Their main findings were that the permeation flux through a tungsten sample appeared independent of sample temperature, but linearly dependent on the implantation flux and increasing with ion energy [16]. No isotope effect between deuterium and tritium was observed, however, there was an isotope effect for transient permeation behaviour, i.e., the time lag until steady-state permeation. This suggested that the activation energy for diffusion is higher for tritium. Another study [77] found that the permeation rate is inversely proportional to the specimen thickness and does not depend on the grain structure of the tungsten sample.

So far, there have not been any studies into differences or contributing factors between gas-driven and plasma-driven permeation. It is important to realise this, as results obtained for one type of permeation may not be applicable to the other.

4.7. Irradiation effects

Realistic irradiation conditions are difficult to replicate, with neutron irradiation not feasible in many experimental environments. Instead, electron, proton and ion irradiation have been used to study irradiation effects on the hydrogen permeation rate.

Studies [78] and [79] looked at the effect of irradiation on grain size, and whether this affected the permeation rate afterwards. It was found that irradiation of an Er_2O_3 coating deposited on F82H up to 1 dpa with Fe^{3+} ions led to the increase in grain size and reduced the permeation rate above 500 °C [78]. Similarly, Y_2O_3 coatings irradiated with Fe^{+} ions up to 1 dpa displayed a different grain structure, leading to a deuterium permeation up to 390 times lower than the unirradiated sample [79].

Comparable results were reported in [22], testing Al_2O_3 on Eurofer-97 under electron irradiation on the permeate side. The deuterium permeation rate decreased by 10–15 % when the irradiation was started. Using the same setup, the authors of [80] did not find any structural changes after the electron irradiation, concluding that the radiation field affected the permeation only dynamically, with the permeation rate recovering to its original value when irradiation is stopped. This was confirmed by an observed reduction in deuterium absorption during irradiation.

Using the same apparatus, the permeation through nickel was investigated under electron irradiation [81]. It was shown here that the permeation increases as a result of the increase in temperature due to the irradiation, as can be expected. Regulating the temperature of the sample during irradiation to remain constant resolved the increase in permeation. Other experiments, as early as 1997 [11], found that simultaneously irradiating a MANET II sample with protons enhances the permeation rate, possibly due to ionisation of the gas on the upstream side.

The effect of gamma radiation has not been studied widely; [82] described the study of deuterium permeation through palladium, platinum and 316 L stainless steel under gamma irradiation. It was found that the permeation increased by approximately 1 %, but this was most likely due to the temperature increase caused by the radiation, as opposed to any structural effects.

These results suggest that the effect of irradiation strongly depends on the sample and coating material, and that various competing effects are at play. As irradiation experiments have been limited in number, no conclusions can be drawn yet on the effect of irradiating species or ion energy. Furthermore, the extent to which these results are comparable to neutron irradiation is still unknown, with earlier work finding a surprisingly low PRF when testing coatings in the High Flux Reactor (HFR) in Petten [30]. These experiments are discussed further in Section 5.

4.8. Contamination, oxidation, and evolution of coatings

Apart from the characteristics of a coating when applied (as discussed in Section 3.3), another important factor to consider is the evolution of the coating; how its performance is affected by consecutive exposures or heating cycles. The effect of exposure to oxygen was already discussed in Section 4.4.

The effect of exposing a F28H steel sample to air, both on the upstream and downstream side, was studied [83,84] and a numerical model was fitted to the permeation curves obtained, both for clean and

contaminated samples. It was found that the time lag is longer and that the permeation flux is lower for contaminated samples, as the contamination reduces the dissociation and recombination rates.

The effect of oxidation reducing the permeation rate was described in [85], repetitively testing deuterium permeation through MANET II with an aluminium oxide coating. The permeation rate eventually dropped by a factor 10^4, due to either a better adherence of the coating to the substrate or the formation of oxides in small cracks in the coating, due to small impurities of O_2 and H_2O present in the deuterium gas.

The effect of oxidation on titanium coatings was investigated [18] using coatings consisting of TiN-TiC with either SiO_2 or TiN on the outside. It was found that both TiN and SiO_2 improved the oxidation resistance of TiC, but SiO_2 did this to a larger extent.

When studying deuterium permeation through samples coated with erbium oxide, it was observed that the pressure exponent for uncoated samples changed from around 0.5 below 723 K to closer to 0.6 above 773 K, while the exponent for coated samples remained constant. This was due to oxidation of the coating, changing the permeation process from diffusion limited to more surface limited [44]. This work was followed by a study of two-layer Er_2O_3 coatings, with either a Fe or Er layer on top [46]. During the deuterium permeation experiments the Fe layer oxidised, enhancing its PRF, while the Er layer oxidised and merged with the Er_2O_3 layer underneath, displaying a similar PRF as a single Er_2O_3 coating. Further work on Er_2O_3 coatings on F82H suggested that crystallisation, started during the formation of the coating, is completed during experiments where the sample is heated to 823 K, further increasing the PRF of the coating [21].

Exploiting the in-situ formation of coatings on Eurofer was researched in [86], by passing a mixture of Ar, water and H_2 over the sample. The effectiveness of this method depended heavily on the ratio of H_2 and H_2O, with a maximum PRF of 30 obtained for a ratio H_2:H_2O of 25:1 only.

In addition to the interaction with oxygen, hydrogen gases themselves can also interact with the coating; it has been observed in [45] that at the start of an experiment the deuterium flux would decrease due to trapping. Further, amorphous SiC coatings on F82H degraded during measurements at 823 K due to crack formation.

The effect of corrosion, especially by materials such as LiPb, will be discussed in the next section.

5. Experiments using breeder materials

A select number of studies have tested either the influence of breeder materials such as LiPb on the effectiveness of anti-permeation coatings, or the performance of coatings when this breeder material was subject to neutron irradiation and generated tritium.

Tritium permeation rates through bare 1 mm thick iron samples and similar iron samples covered by an 8.5 mm layer of molten LiPb have been studied in [87]. The permeation flux was halved in the presence of the LiPb layer. In contrast, LiPb layers have been shown to reduce the permeation of hydrogen by two orders of magnitude, hence differences between the hydrogen isotopes' transport properties cannot be ignored.

The effect of immersion in LiPb on the effectiveness of an erbium zirconium oxide layer was also investigated in [88]. It was found that the coating has a good corrosion resistance when immersed in LiPb up to 550 °C, with visible damage occurring at 600 °C. However, the effect that this immersion has on the PRF of the coating was not investigated.

Between 1990 and 2014, several publications described the studies performed in the High Flux Reactor (HFR) in Petten, part of the LIBRETTO and EXOTIC experimental programmes. Capsules containing breeder materials were irradiated by neutrons, with the tritium generated permeating through the wall of the capsules and being detected. By measuring these different tritium fluxes the effectiveness of different coatings in an irradiation environment could be determined.

No tritium release from capsules filled with LiPb was observed at temperatures below 267 °C [89]. It was found that an Al_2O_3 coating increased the residence time of tritium by a factor of 4. When both TiC and Al_2O_3 coatings were tested [90], surprisingly low permeation reduction factors between 3 and 15 were found. Several years later the tritium permeation of tritium generated from Li_2TiO_3 pebbles was studied [65]. A copper interlayer between two steel tubes and an aluminium oxide coating deposited on the outside of the tube were tested for their permeation reduction performance. Both showed no increase in tritium permeation during the experiment, suggesting that they did not deteriorate due to tritium permeation.

Across all these experiments, the diffusion constant of tritium was determined to be one order of magnitude lower than literature data predicted. This suggests that irradiation can slow down diffusion [91] possibly due to enhanced trapping at irradiation induced defects. Further testing on Eurofer tubes filled with Li_2TiO_3 pebbles and irradiated up to 1.2 dpa showed that the resulting tritium permeation was in the diffusion limited regime [92].

Another experiment, performed with LiPb in the IVG.1 M (Water-cooled Heterogeneous Research - Modernised) reactor in Kazakhstan, tested a coating of Cr_2O_3-SiC [93]. PRF values of 30 and 292 for tritium were determined at 500 °C and 600 °C, respectively. The same coating, tested out-of-pile for deuterium, had PRFs of 45 and 307 at the same temperatures. This increase in PRF could be caused by the decrease in micro-defects in the coating due to grain growth or due to its self-healing abilities at this higher temperature.

The main observations from these experiments, involving tritium generated in breeder materials under neutron irradiation, are that the PRF values obtained are low compared to the ones found in literature, while diffusion can be slowed down compared to literature data. This suggests that further research into these factors is necessary, and testing of anti-permeation coatings under neutron irradiation is required.

6. Experimental design and operation

A basic experimental method for measuring permeation rates was explained in Section 2.8. However, there are several practical implications that need to be considered when designing a permeation experiment, that this section will elucidate on.

6.1. Geometry

Section 2.8 describes a setup that derives the permeation rate from the pressure increase on the downstream side of the sample. However, there are several drawbacks related to this method; the high loading pressure (10^4 – 10^5 Pa) that is needed to obtain a measurable pressure increase on the permeate side, the possibility of back diffusion and the mechanical loads acting on the membrane from the pressure difference between both sides [94].

Alternatively, a gas release experiment can be performed where a sample is loaded with hydrogen under a certain temperature. The sample chamber is evacuated, and the desorption rate of the hydrogen is determined. Tests can be run with and without the sample to determine the background desorption rate [94].

Both methods are marred by a difficulty to account for losses to the surrounding structures [94], which is enhanced by the geometry of flat sample holders for disc shapes; only one side of the upstream chamber is made of the material to investigate, implying that >50 % of the chamber walls is *not* of interest. Permeation through these walls will lead to losses to the environment, especially when the whole sample holder is heated to elevated temperatures. This issue is exacerbated when coatings with a high PRF are tested; the walls will be several orders of magnitude more permeable than the sample itself.

This issue could be resolved by using a tubular geometry instead. There have been various permeation setups using a tube as sample holder [17,20,33], where the gas is inserted in the inner tube, permeating into an outer tube or containment. One advantage of this geometry is the large fraction of surface area that acts as sample; only the ends of

the tube provide possible routes for unwanted permeation. However, as flat samples are easier to manufacture than tubes, especially when coatings are applied, a flat geometry is adopted in several cases, allowing for easier production of samples and testing of various materials and coatings.

Other issues arise due to the need to evacuate the downstream side of the sample. Here the walls will absorb hydrogen during the experiments, which will off-gas when the chamber is evacuated. Achieving a low and constant pressure here is only possible after pumping for a considerable amount of time. In [23] it was observed that this retained gas caused the pressure to increase faster than expected at the start of an experiment, especially in the case of low-pressure experiments. This issue was addressed in [95], when the authors tested a new design of sample holder with a thin-walled inset, to retain less hydrogen and release this faster than a thick-walled sample holder would do. After 24 h, a 160 times smaller outgassing flux was observed.

Further practical questions arise due to the need to enclose the sample in a sample holder. Examples include whether the temperature of the sample can be determined accurately if the sample holder is heated instead of the sample itself and whether the sample is heated uniformly. Other considerations include whether the process gas needs to be heated itself or whether it will reach the desired temperature by being in contact with the heated sample holder. Moreover, tube samples are usually welded into place [17,73,75]. Machining and welding a material will affect its surface finish, which could influence hydrogen permeation rates through it. These questions should be considered carefully when designing a sample holder, and when comparing results obtained by different setups with each other.

6.2. The chronological order of experimental operations

There have been various experiments performed where the experimental conditions were changed stepwise, obtaining several results for the same sample. An example of starting the permeation tests at the highest temperature, after which the temperature was lowered in steps, is described in [83,44], the pressure of deuterium gas was varied, starting with a low pressure and doubling this pressure three consecutive times. Notably, the same authors published a paper 2 years later describing how the deuterium pressure was decreased several times using the same sample [45]. However, no comparison was made between the two studies, and the reasons for adopting this pressure sequence were not shared. The only recommendation that can be made here is to consider potential memory effects of detection equipment; in this case it is advisable to start with a lower permeation rate or concentration, to not interfere with later measurements.

When working with tritium, contamination of equipment between experiments is a major issue. It is therefore recommended that various purge and bake-out cycles are performed between experiments, to aid any residual tritium off-gassing. Further, experiments with low inventories of tritium should be performed first. This does not only reduce operational risks, operators gaining experience on low-inventory operations before moving on to high-inventory ones, but also ensures that background signals arising from contamination do not exceed the measurement signal.

6.3. Flowing gases

Permeation in fusion power plants will rarely occur in static systems at high temperatures; most subsystems contain flowing gases or liquids, and in the case of high temperatures there will most likely be a flowing coolant medium present as well. As such, experiments involving flowing gases have gained interest lately, exploring permeation processes in more realistic conditions.

Experiments with flowing gases have typically been performed in a double-tube configuration, consisting of two concentric tubes. The hydrogen isotopes are inserted in either the inner or outer tube, and the concentration of the gases are monitored. Inert gases such as helium and argon are commonly used with typical flow rates in the range 2 – 12 L/hr, with variation possible between up- and downstream sides of the sample.

For example, in [17] the permeation of tritium from a sealed tube into a flowing argon stream was studied. The tritium concentration of this gas was measured with an ionisation chamber. The authors mentioned that the gas rate had to be adjusted to ensure the ionisation chamber was working correctly but did not study the effect of a varying flow rate on the permeation rate.

In some experiments flat disc samples instead of tubular samples have been used, with the gas flowing through both chambers. Examples are [61] working with deuterium and a quadrupole mass spectrometer, and [63] using tritium and performing analysis with an ionisation chamber. The authors of [62] also used a flat sample holder with flowing gases both upstream and downstream, with flow rates of 3 and 12 L/hr, respectively. The experimental setup was equipped with both ionisation chambers and a catalyst bed and bubbler setup, used to test the agreement between the ionisation chamber measurements and liquid scintillation detection of tritium. The same rig was also used to test the transport coefficients of tritium through liquid lithium [87].

6.4. Detection methods

The detection method that can be deployed in a permeation rig depends on the setup of the rig (non-flowing or flowing gases) and whether protium, deuterium or tritium permeation is studied. Here it matters only whether the downstream side is flowing or not, the upstream side does not influence the choice of detection technology.

In a non-flowing configuration a pressure rise can be monitored to determine the permeation rate, possibly combined with mass spectrometry (applicable to all hydrogen isotopes and required for co- and counter permeation measurements) or ionisation chambers (tritium only) to determine the composition of the gas. However, measuring a pressure increase is not feasible when the gases are flowing, as the permeate partial pressure will be negligible compared to the total pressure.

A flowing configuration lends itself to other measurement techniques, even though ionisation chambers and quadrupole mass spectrometers are also valid options. Examples include a gas chromatograph as described in [33] or bubblers combined with liquid scintillation in [62,87]. It is difficult to adopt a static rig to incorporate these measurement technologies as they change the composition of the gases that flow through; gas chromatography separates out different components while an oxidising catalyst converts HT and T_2 gas into tritiated water. This contrasts with ionisation chambers where gas can be recirculated through the chamber as it leaves the device unaltered.

When deciding on which detection method to use, it is important to consider whether it is necessary to distinguish between different hydrogen isotopes, in case co- and counter permeation is studied. For example, a gas chromatograph or mass spectrometer can distinguish between hydrogen isotopes, while deuterium cannot be detected using liquid scintillation.

6.5. Difficulties induced by the coating

As mentioned in Section 2.4, the surface-limited regime applies to small pressure differences between the up- and downstream side of the metal. In future systems such as breeder blankets the pressure gradient through the permeation barrier is expected to be small, implying a surface-limited permeation process.

However, a smaller difference in pressures between either side of the sample implies a lower permeation rate. Adding a coating reduces the permeation even further, approaching the detection limit [28]. Other sources of hydrogen such as background outgassing may exceed the amounts permeating. This explains why most experiments operate in the

diffusion-limited regime. As the name implies, surface effects become more important in the SLR, and with it the characteristics of the coating such as grain boundaries. This can dramatically change the expected permeation behaviour at different pressures, and extrapolation to lower pressures is unreliable as a result.

Further, the lower the permeability of the substrate, the more difficult it is to determine the PRF of the system where a coating is applied to this substrate. In many cases the temperature must be raised to determine a reliable PRF. The effect of temperature on the distinction between DLR and SLR has not been investigated yet, but [25] observed that the pressure exponent of a Y_2O_3 coating changed from 0.469 to 0.741 when heated from 500 °C to 650 °C. This is a significant increase over a relatively small temperature interval.

Moreover, there is usually a discrepancy between a calculated high PRF value and much lower measured value [28]. This can be caused by leakage through microscopic and nano-sized imperfections within the permeation barrier itself. It is therefore recommended that detection technologies are used with low limits of detection, and off-gassing is reduced by either design of the sample holder or extensive bake-out procedures.

6.6. Compatibility of different design options

A summary of the compatibilities of combinations of different experimental design choices that have been discussed in this section is shown in Table 1. It needs to be noted that:

- A flowing / non-flowing setup concerns the downstream side of the sample only
- The geometry does not determine whether flowing gases are used
- When multiple isotopes are used, determining the permeation rate from a pressure increase or a method that can only detect tritium is not a valid option. However, it could be suitable if used in combination with another detection method. This is shown using a † in Table 1.
- Liquid scintillation and gas chromatography could both be installed in the same rig, but could not analyse the same gas stream, as gas needs to be diverted to either at set intervals
- Pressure measurements are not useful for flowing setups, and neither are gas chromatography and liquid scintillation for non-flowing setups.

The following acronyms for detection methods are used: P = pressure, IC = ionisation chamber, MS= mass spectrometry, GC = gas chromatography, LSC = liquid scintillation counting.

7. Summary and outlook

This paper has described the many factors that affect the permeation of hydrogen isotopes through metals, and how these can affect the performance of anti-permeation coatings. It has highlighted constraints that experimental researchers face when studying the transport of hydrogen isotopes through metals.

Scientific experiments are limited in their ability to simulate a real fusion reactor environment in several ways:

Table 1
overview of compatibilities between different experimental design decisions.

		Setup		Isotopes used		
		No Flow	Flow	no T	T	multiple
Detection method	P	×	✓	✓	✓	×†
	IC	✓	✓	×	✓	×†
	MS	✓	✓	✓	✓	✓
	GC	✓	×	✓	✓	✓
	LSC	✓	×	×	✓	×†

- The pressure that the experiments are operated at give rise to the diffusion limited regime, not the surface limited regime as expected in breeder blankets. This implies that surface effects cannot be observed properly and may be overlooked.
- Temperature gradients through materials are not frequently investigated, and the performance of coatings at high temperature is difficult to study in a lab environment.
- The effects of flow rate on permeation are not investigated widely although this may have an influence on the permeation rate. When flowing gases are used in experiments the flow rates are generally small compared to fusion fuel cycle conditions.
- The effect that the coolant has on the permeation rate has not been investigated, as theory suggests there will be no effect. However, results from other scientific areas suggest the composition of the downstream medium could have an effect and tests are required to provide more information on this. The permeation into water has rarely been studied, while water coolants will be used in fusion fuel cycles, especially in the steam generator and are expected to act as tritium sinks.
- Although there may not be an observable difference between flat and tubular geometries when the permeation rate is concerned, there are still challenges to be overcome in applying coatings to the inside of pipes, which would be the optimal location for permeation reduction.
- Some locations in the fuel cycle will be subject to plasma driven permeation or a combination of gas- and plasma driven permeation, while almost all experiments have only studied gas driven permeation. How these two are related and whether results obtained with gas driven permeation can be applied to plasma driven permeation and vice versa is still not understood.
- Irradiation can cause competing effects such as changing the grain size or increasing the sample temperature. There is very limited data on neutron irradiation effects or how these effects related to proton, electron, or ion irradiation.
- Coatings will get contaminated and will trap large amounts of hydrogen isotopes during their lifetime. However, the materials will be in place in the fuel cycle for much longer than we can test them for. Coating longevity and durability is uncertain, especially for powerplant lifetimes and in fusion relevant conditions. For this purpose, exposing material samples to fusion reactor conditions is recommended, for example the development of a 14 MeV neutron source to test breeder blanket concepts as explained in [96].

It is therefore important when designing experiments to strive to study these factors and to replicate fusion-relevant conditions as closely as possible. However, the design of the experiment has a profound effect on the results that can be obtained:

- The design of the sample holder determines what fraction of the walls can give rise to unwanted permeation. As such, a tubular sample geometry or a design with thin walls would be preferred.
- Requiring a vacuum on the downstream side leads to the issue of off-gassing of retained hydrogen in the walls. Memory and contamination effects need to be considered before deciding on the order in which experiments are performed.
- Using flowing gases allows for the use of other detection technologies and removes the need to maintain a vacuum on the downstream side. However, when using tritium this leads to a large amount of contamination.
- The setup of the experiment and which hydrogen isotopes are being used determines which detection technology is applicable. This is an important factor to consider, especially when low permeation rates in the surface limited regime are to be detected.
- Isotope effects in materials used for substrates do exist, but their magnitude seems to depend on several factors and can be different for different materials. It is recommended that tritium is used where

possible, as extrapolation from deuterium results may not be accurate.

To conclude, the main challenges and open questions in anti-permeation coatings research are:

- The use of tritium, imposing a higher level of complexity to experimental design and safety considerations and leading to contamination of equipment.
- The effects of irradiation, especially in-situ neutron irradiation.
- Finding the optimal application method for a coating, depending on the substrate geometry, yielding a coating with the desired grain structure, thickness, and surface finish while minimising defects. Developing coatings that are resistant to corrosion and adhere to the substrate under challenging conditions and thermal cycling.

7.1. Outlook

To address some of the experimental limitations and design challenges, we have designed a permeation rig at UKAEA studying the permeation of tritium through a sample into a flowing gas stream. This experiment will be located in the JET Active Gas Handling System, benefiting from >30 years of experience in handling tritium. Due to its location, the experimental rig can handle several TBq's of tritium at one time. The flow rate of the downstream gas is kept low to limit tritium contamination but can be varied to study any effect on the permeation rate. Two separate sample holders are being developed with different geometries; a concentric tube sample holder will be used to study the tritium permeation rate in a realistic geometry and to limit unwanted permeation, while a flat sample holder is being developed to test readily available coated samples, allowing for easy changing over of samples and testing a wide variety of materials in a short time frame. As primary detection method liquid scintillation will be used, to deliver the most accurate results. There will also be an ionisation chamber installed and a residual gas analyser, with the latter able to perform qualitative analysis on the permeation of inactive hydrogen isotopes. Preliminary results are expected by the end of 2026.

CRediT authorship contribution statement

Teuntje Tijssen: Formal analysis, Conceptualization, Data curation, Writing – original draft.

Declaration of competing interest

The authors declare that they have no known competing financial interests or personal relationships that could have appeared to influence the work reported in this paper.

Acknowledgements

This work has been carried out within the framework of the EUROfusion Consortium, funded by the European Union via the Euratom Research and Training Programme (Grant Agreement No 101052200 — EUROfusion). Views and opinions expressed are however those of the author(s) only and do not necessarily reflect those of the European Union or the European Commission. Neither the European Union nor the European Commission can be held responsible for them.

Data availability

No data was used for the research described in the article.

References

[1] Y. Xu, Z.S. Wu, L.M. Luo, X. Zan, X.Y. Zhu, Q. Xu, Y.C. Wu, Transport parameters and permeation behavior of hydrogen isotopes in the first wall materials of future fusion reactors, Fusion Eng. Des. 155 (2020) 1–10, https://doi.org/10.1016/j.fusengdes.2020.111563.
[2] T. Chikada, Ceramic coatings for fusion reactors, in: comprehensive nuclear materials, Elsevier Ltd (2020) 274–283, https://doi.org/10.1016/b978-0-12-803581-8.11674-1.
[3] W. Tyson, Hydrogen in metals, Can. Metall. Q. 18 (1979) 1–11, https://doi.org/10.1179/cmq.1979.18.1.1.
[4] G.W. Hollenberg, E.P. Simonen, G. Kalinin, A. Terlain, Tritium /hydrogen barrier development, Fusion Eng. Des. 28 (1995) 190–208, https://doi.org/10.1016/0920-3796(95)90039-X.
[5] A. Santucci, M. Incelli, L. Noschese, C. Moreno, F. Di Fonzo, M. Utili, S. Tosti, C. Day, The issue of tritium in DEMO coolant and mitigation strategies, Fusion Eng. Des. 158 (2020) 111759, https://doi.org/10.1016/j.fusengdes.2020.111759.
[6] F. Franza, L.V. Boccaccini, D. Demange, A. Ciampichetti, M. Zucchetti, Tritium permeation issues for helium-cooled breeding blankets, in: 2013 IEEE 25th Symposium on Fusion Engineering, SOFE 2013, 2013, pp. 1–6, https://doi.org/10.1109/SOFE.2013.6635335.
[7] D. Demange, L.V. Boccaccini, F. Franza, A. Santucci, S. Tosti, R. Wagner, Tritium management and anti-permeation strategies for three different breeding blanket options foreseen for the European Power Plant Physics and Technology Demonstration reactor study, Fusion Eng. Des. 89 (2014) 1219–1222, https://doi.org/10.1016/j.fusengdes.2014.04.028.
[8] A. Santucci, A. Ciampichetti, D. Demange, F. Franza, S. Tosti, Tritium migration in HCLL and WCLL blankets: impact of tritium solubility in liquid Pb-17Li, IEEE Trans. Plasma Sci. 42 (2014) 1053–1057, https://doi.org/10.1109/TPS.2014.2305759.
[9] R.A. Causey, R.A. Karnesky, C.San Marchi, Tritium barriers and tritium diffusion in fusion reactors, Compr. Nucl. Mater. 4 (2012) 511–549, https://doi.org/10.1016/B978-0-08-056033-5.00116-6.
[10] M. Shimada, Tritium transport in fusion reactor materials, Compr. Nucl. Mater. 6 (2020) 251–273, https://doi.org/10.1016/b978-0-12-803581-8.11754-0.
[11] F. Wedig, P. Jung, Effects of irradiation and implantation on permeation and diffusion of hydrogen isotopes in iron and martensitic stainless steel, J. Nucl. Mater. 245 (1997) 138–146, https://doi.org/10.1016/S0022-3115(97)00014-7.
[12] Y. Ebisuzaki, W.J. Kass, M. O'Keefee, Isotope effects in the diffusion and solubility of hydrogen in nickel, J. Chem. Phys 46 (1967) 1373–1378, https://doi.org/10.1063/1.1840859.
[13] J.K. Baird, E.M. Schwartz, Isotope effect in hydrogen diffusion in metals, Z. Phys. Chem. 211 (1999) 47–68.
[14] M. Urrestizala, J. Azkurreta, N. Alegría, I. Peñalva, Isotope effect of hydrogen and deuterium permeability and diffusivity in fusion reactor materials. A literature review, Fusion Eng. Des. 194 (2023), https://doi.org/10.1016/j.fusengdes.2023.113915.
[15] W.J. Byeon, S.W. Yoon, H. Seo, H.S. Kim, C.H. Lee, S.K. Lee, B.H. Chung, S.J. Noh, Hydrogen-isotope transport in Ti-added reduced activation ferritic/martensitic steel, Fusion Eng. Des. 158 (2020) 111849, https://doi.org/10.1016/j.fusengdes.2020.111849.
[16] H. Nakamura, T. Hayashi, T. Kakuta, T. Suzuki, M. Nishi, Tritium permeation behavior implanted into pure tungsten and its isotope effect, J. Nucl. Mater. 297 (2001) 285–291, https://doi.org/10.1016/S0022-3115(01)00635-3.
[17] F. Yang, X. Xiang, G. Lu, G. Zhang, T. Tang, Y. Shi, X. Wang, Tritium permeation characterization of Al2O3/FeAl coatings as tritium permeation barriers on 321 type stainless steel containers, J. Nucl. Mater. 478 (2016) 144–148, https://doi.org/10.1016/j.jnucmat.2016.06.001.
[18] Z. Yao, J. Hao, C. Zhou, C. Shan, J. Yu, The permeation of tritium through 316L stainless steel with multiple coatings, J. Nucl. Mater. 283–287 (2000) 1287–1291, https://doi.org/10.1016/S0022-3115(00)00349-4.
[19] D. Levchuk, S. Levchuk, H. Maier, H. Bolt, A. Suzuki, Erbium oxide as a new promising tritium permeation barrier, J. Nucl. Mater. 367-370 (2007) 1033–1037, https://doi.org/10.1016/j.jnucmat.2007.03.183. B.
[20] H.G. Yang, Q. Zhan, W.W. Zhao, X.M. Yuan, Y. Hu, Z.B. Han, Study of an iron-aluminide and alumina tritium barrier coating, J. Nucl. Mater. 417 (2011) 1237–1240, https://doi.org/10.1016/j.jnucmat.2011.03.040.
[21] T. Chikada, S. Naitoh, A. Suzuki, T. Terai, T. Tanaka, T. Muroga, Deuterium permeation through erbium oxide coatings on RAFM steels by a dip-coating technique, J. Nucl. Mater. 442 (2013) 533–537, https://doi.org/10.1016/j.jnucmat.2013.05.072.
[22] D. Iadicicco, S. Bassini, M. Vanazzi, P. Munoz, A. Morono, T. Hernandez, I. Garcia-Cortés, F.J. Sánchez, M. Utili, F. Garcia Ferré, F. Di Fonzo, Efficient hydrogen and deuterium permeation reduction in Al2O3 coatings with enhanced radiation tolerance and corrosion resistance, Nucl. Fusion 58 (2018), https://doi.org/10.1088/1741-4326/aadd1d.
[23] V. Nemanič, M. Žumer, J. Kovač, Hydrogen permeability of AISI 316 ITER grade stainless steel, J. Nucl. Mater. 521 (2019) 38–44, https://doi.org/10.1016/j.jnucmat.2019.04.043.
[24] A. Aiello, I. Ricapito, G. Benamati, R. Valentini, Hydrogen isotopes permeability in Eurofer 97 martensitic steel, Fusion Sci. Technol. 41 (2002) 872–876, https://doi.org/10.13182/fst41-872.
[25] L. Wang, C. Zhu, C. Liang, Y. Feng, B. Gong, Y. Wang, J. Wei, Y. Wu, N. Liu, J. Yang, Preparation and characterization of Al2O3/Y2O3 multilayer coatings as tritium permeation barrier, Mater. Res. Express 6 (2019).

[26] P. Pereslavtsev, F.A. Hernández, G. Zhou, L. Lu, C. Wegmann, U. Fischer, Nuclear analyses of solid breeder blanket options for DEMO: status, challenges and outlook, Fusion Eng. Des. 146 (2019) 563–567, https://doi.org/10.1016/j.fusengdes.2019.01.023.
[27] E. Serra, G. Benamati, O.V. Ogorodnikova, Hydrogen isotopes transport parameters in fusion reactor materials, J. Nucl. Mater. 255 (1998) 105–115, https://doi.org/10.1016/S0022-3115(98)00038-5.
[28] V. Nemanič, Hydrogen permeation barriers: basic requirements, materials selection, deposition methods, and quality evaluation, Nucl. Mater. Energy 19 (2019) 451–457, https://doi.org/10.1016/j.nme.2019.04.001.
[29] T. Tanabe, Review of hydrogen retention in tungsten, Phys Scr T 159 (2014), https://doi.org/10.1088/0031-8949/2014/T159/014044.
[30] R.A. Causey, R.A. Karnesky, C.San Marchi, Tritium Barriers and Tritium Diffusion in Fusion Reactors, Elsevier Inc., 2012, https://doi.org/10.1016/B978-0-08-056033-5.00116-6.
[31] P. Calderoni, P. Humrickhouse, R. Pawelko, M. Shimada, P. Winston, Tritium permeability of Incoloy 800H and Inconel 617, Ida. Natl. Lab. INL/EXT-11 (2011), https://doi.org/10.2172/1033884.
[32] E.H. Van Deventer, V.A. Maroni, Hydrogen permeation characteristics of some austenitic and nickel-base alloys, J. Nucl. Mater. 92 (1980) 103–111, https://doi.org/10.1016/0022-3115(80)90146-4.
[33] M. Nishikawa, T. Shiraishi, Y. Kawamura, T. Takeishi, Permeation rate of hydrogen isotopes through palladium- silver alloy, J. Nucl. Sci. Technol 33 (1996) 774–780, https://doi.org/10.1080/18811248.1996.9732002.
[34] D. Levchuk, F. Koch, H. Maier, H. Bolt, Deuterium permeation through Eurofer and α-alumina coated Eurofer, J. Nucl. Mater. 328 (2004) 103–106, https://doi.org/10.1016/j.jnucmat.2004.03.008.
[35] D. Levchuk, H. Bolt, M. Dobeli, S. Eggenberger, B. Widrig, J. Ramm, Al-Cr-O think films as an efficient hydrogen barrier, Surf. Coat. Technol 202 (2008) 5043–5047, https://doi.org/10.1016/j.surfcoat.2008.05.012.
[36] J. Engels, A. Houben, P. Hansen, M. Rasinski, C. Linsmeier, Influence of the grain structure of yttria thin films on the hydrogen isotope permeation, Int. J. Hydrog. Energy 43 (2018) 22976–22985, https://doi.org/10.1016/j.ijhydene.2018.09.191.
[37] A. Pisarev, I. Tsvetkov, S. Yarko, Hydrogen permeation through membranes with cracks in protection layer, Fusion Eng. Des. 82 (2007) 2120–2125, https://doi.org/10.1016/j.fusengdes.2007.04.005.
[38] T. Chikada, A. Suzuki, T. Kobayashi, H. Maier, T. Terai, T. Muroga, Microstructure change and deuterium permeation behavior of erbium oxide coating, J. Nucl. Mater. 417 (2011) 1241–1244, https://doi.org/10.1016/j.jnucmat.2010.12.283.
[39] Y. Hatano, K. Zhang, K. Hashizume, Fabrication of ZrO 2 coatings on ferritic steel by wet-chemical methods as a tritium permeation barrier, Phys. Scr. T T145 (2011), https://doi.org/10.1088/0031-8949/2011/T145/014044.
[40] T. Chikada, A. Suzuki, C. Adelhelm, T. Terai, T. Muroga, Surface behaviour in deuterium permeation through erbium oxide coatings, Nucl. Fusion 51 (2011), https://doi.org/10.1088/0029-5515/51/6/063023.
[41] R. Checchetto, M. Bonelli, L.M. Gratton, A. Miotello, A. Sabbioni, L. Guzman, Y. Horino, G. Benamati, Analysis of the hydrogen permeation properties of TiN-TiC bilayers deposited on martensitic stainless steel, Surf. Coat. Technol 83 (1996) 40–44, https://doi.org/10.1016/0257-8972(96)02851-4.
[42] S. Horikoshi, J. Mochizuki, Y. Oya, T. Chikada, Deuterium permeation and retention behaviors in erbium oxide-iron multilayer coatings, Fusion Eng. Des. 124 (2017) 1086–1090, https://doi.org/10.1016/j.fusengdes.2017.03.123.
[43] G.A. Esteban, A. Peña, I. Urra, F. Legarda, B. Riccardi, Hydrogen transport and trapping in EUROFER'97, J. Nucl. Mater. 367-370 A (2007) 473–477, https://doi.org/10.1016/j.jnucmat.2007.03.114.
[44] T. Chikada, A. Suzuki, Z. Yao, D. Levchuk, H. Maier, T. Terai, T. Muroga, Deuterium permeation behavior of erbium oxide coating on austenitic, ferritic, and ferritic/martensitic steels, Fusion Eng. Des. 84 (2009) 590–592, https://doi.org/10.1016/j.fusengdes.2008.12.030.
[45] T. Chikada, A. Suzuki, T. Terai, Deuterium permeation and thermal behaviors of amorphous silicon carbide coatings on steels, Fusion Eng. Des. 86 (2011) 2192–2195, https://doi.org/10.1016/j.fusengdes.2011.01.036.
[46] T. Chikada, A. Suzuki, F. Koch, H. Maier, T. Terai, T. Muroga, Fabrication and deuterium permeation properties of erbia-metal multilayer coatings, J. Nucl. Mater. 442 (2013) S592–S596, https://doi.org/10.1016/j.jnucmat.2013.03.084.
[47] J. Matějíček, J. Veverka, V. Nemanič, L. Cvrček, F. Lukáč, V. Havránek, K. Illková, Characterization of less common nitrides as potential permeation barriers, Fusion Eng. Des. 139 (2019) 74–80, https://doi.org/10.1016/j.fusengdes.2018.12.056.
[48] Z. Chen, X. Hu, M. Ye, B.D. Wirth, Deuterium transport and retention properties of representative fusion blanket structural materials, J. Nucl. Mater. 549 (2021) 152904, https://doi.org/10.1016/j.jnucmat.2021.152904.
[49] T. Hernández, A. Moroño, F.J. Sánchez, C. Maffiotte, M.A. Monclús, R. González-Arrabal, Study of deuterium permeation, retention, and desorption in SiC coatings submitted to relevant conditions for breeder blanket applications: thermal cycling effect under electron irradiation and oxygen exposure, J. Nucl. Mater. 557 (2021), https://doi.org/10.1016/j.jnucmat.2021.153219.
[50] Y. Shimizu, H. Fujiwara, K. Shirota, W. Matsuura, T. Ito, K. Do-Duy, T. Chikada, Fabrication and characterization of enamel coating as a promising hydrogen and oxygen diffusion barrier, Fusion Eng. Des. 204 (2024) 114506, https://doi.org/10.1016/j.fusengdes.2024.114506.
[51] J. Engels, A. Houben, M. Rasinski, C. Linsmeier, Hydrogen saturation and permeation barrier performance of yttrium oxide coatings, Fusion Eng. Des. 124 (2017) 1140–1143, https://doi.org/10.1016/j.fusengdes.2017.01.058.
[52] K. Zhang, Y. Hatano, Preparation of Mg and Al phosphate coatings on ferritic steel by wet-chemical method as tritium permeation barrier, Fusion Eng. Des. 85 (2010) 1090–1093, https://doi.org/10.1016/j.fusengdes.2010.02.012.
[53] S.K. Lee, H.S. Kim, S.J. Noh, J.H. Han, Hydrogen permeability, diffusivity, and solubility of SUS 316L stainless steel in the temperature range 400 to 800 °C for fusion reactor applications, J. Korean Phys. Soc. 59 (2011) 3019–3023, https://doi.org/10.3938/jkps.59.3019.
[54] F. Liu, H. Zhou, X.C. Li, Y. Xu, Z. An, H. Mao, W. Xing, Q. Hou, G.N. Luo, Deuterium gas-driven permeation and subsequent retention in rolled tungsten foils, J. Nucl. Mater. 455 (2014) 248–252, https://doi.org/10.1016/j.jnucmat.2014.06.005.
[55] S. Rai, P.A. Rayjada, P.B. Dhorajiya, R.B. Patel, S.K. Sharma, A. Sircar, R. Bhattacharyay, Deuterium permeation studies through bare and Er2O3 coated SS 316L, Fusion Eng. Des. 206 (2024) 114587, https://doi.org/10.1016/j.fusengdes.2024.114587.
[56] F. Yang, X. Xiang, C. Chen, L. Hu, C. Ma, G. Zhang, Y. Song, Formation, characterization and deuterium permeation of Al2O3/Fe-Al layers on SS-316L surface, Fusion Eng. Des. 209 (2024), https://doi.org/10.1016/j.fusengdes.2024.114735.
[57] F. Hernández, P. Pereslavtsev, Q. Kang, P. Norajitra, B. Kiss, G. Nádasi, O. Bitz, A new HCPB breeding blanket for the EU DEMO: evolution, rationale and preliminary performances, Fusion Eng. Des. 124 (2017) 882–886, https://doi.org/10.1016/j.fusengdes.2017.02.008.
[58] M. Malo, F.J. Valle, F.M. Jiménez, A. Moroño, E.R. Hodgson, C. Moreno, Hisotope thermo-diffusion in structural materials, Fusion Eng. Des. 124 (2017) 924–927, https://doi.org/10.1016/j.fusengdes.2017.01.012.
[59] H. Zhang, A. Ying, M.A. Abdou, Integrated simulation of tritium permeation in solid breeder blankets, Fusion Eng. Des. 85 (2010) 1711–1715, https://doi.org/10.1016/j.fusengdes.2010.05.018.
[60] V. Violante, S. Tosti, C. Sibilia, F. Felli, S. Casadio, C. Alvani, Tritium inventory and permeation in the ITER breeding blanket, Fusion Eng. Des. 49 (2000) 697–701, https://doi.org/10.1016/S0920-3796(00)00173-3.
[61] D. Klimenko, F. Arbeiter, V. Pasler, G. Schlindwein, A. von der Weth, K. Zinn, Definition of the Q-PETE experiment for investigation of hydrogen isotopes permeation through the metal structures of a DEMO HCPB breeder zone, Fusion Eng. Des. 136 (2018) 563–568, https://doi.org/10.1016/j.fusengdes.2018.03.024.
[62] M. Shimada, R.J. Pawelko, Tritium permeability measurement in hydrogen-tritium system, Fusion Eng. Des. 129 (2018) 134–139, https://doi.org/10.1016/j.fusengdes.2018.02.033.
[63] H. Zhang, A. Ying, M. Abdou, M. Shimada, B. Pawelko, S. Cho, Characterization of tritium isotopic permeation through ARAA in diffusion limited and surface limited regimes, Fusion Sci. Technol. 72 (2017) 416–425, https://doi.org/10.1080/15361055.2017.1333826.
[64] N.N. Zulkefli, M.S. Masdar, W.R.W. Isahak, J. Jahim, E.H. Majlan, S.A.M. Rejab, C. C. Lye, Mathematical modelling and simulation on the adsorption of Hydrogen sulfide (H2S) gas, IOP. Conf. Ser. Mater. Sci. Eng 206 (2017), https://doi.org/10.1088/1757-899X/206/1/012069.
[65] A.J. Magielsen, K. Bakker, C. Chabrol, R. Conrad, J.G. Van der Laan, E. Rigal, M. P. Stijkel, In-pile performance of a double-walled tube and a tritium permeation barrier, J. Nucl. Mater. 307–311 (2002) 832–836, https://doi.org/10.1016/S0022-3115(02)01305-3.
[66] M.J. Tang, R.A. Cox, M. Kalberer, Compilation and evaluation of gas phase diffusion coefficients of reactive trace gases in the atmosphere: volume 1. Inorganic compounds, Atmos. Chem. Phys 14 (2014) 9233–9247, https://doi.org/10.5194/acp-14-9233-2014.
[67] H. Amandusson, L.-G. Ekedahl, H. Dannetun, The effect of CO and O2 on hydrogen permeation through a palladium membrane, Appl. Surf. Sci 153 (2000) 259–267, https://doi.org/10.1016/S0169-4332(99)00357-8.
[68] R.G. Hickman, Some problems associated with tritium in fusion reactors, in: Texas Symposium on the Technology of Controlled Thermonuclear Fusion Experiments and the Engineering Aspects of Fusion Reactors, Austin, Texas, 1972: pp. 1–36. https://doi.org/10.2172/4605890.
[69] K. Kizu, A. Pisarev, T. Tanabe, Co-permeation of deuterium and hydrogen through Pd, J. Nucl. Mater. 289 (2001) 291–302, https://doi.org/10.1016/S0022-3115(01)00428-7.
[70] K. Kizu, T. Tanabe, Counter-diffusion and counter-permeation of deuterium and hydrogen through palladium, J. Nucl. Mater. 258–263 (1998) 1133–1137, https://doi.org/10.1016/S0022-3115(98)00393-6.
[71] K. Kizu, T. Tanabe, Deuterium permeation through metals under hydrogen counter flow, J. Nucl. Mater. 266 (1999) 561–565, https://doi.org/10.1016/S0022-3115(98)00589-3.
[72] S.J. Hendricks, E. Carella, D. Jimenez, J.M. Garcia, J. Molla, Design of a multi-isotopic co- and counter-permeation experiment, Fusion Eng. Des. 175 (2022) 112991, https://doi.org/10.1016/j.fusengdes.2021.112991.
[73] T. Hayashi, H. Nakamura, K. Isobe, K. Kobayashi, M. Oyaizu, T. Yamanishi, Y. Oya, K. Okuno, Hydrogen isotope permeation from cooling water through various metal piping, Fusion Eng. Des. 87 (2012) 1333–1337, https://doi.org/10.1016/j.fusengdes.2012.03.009.
[74] H. Nakamura, M. Nishi, Experimental evaluation of tritium permeation through stainless steel tubes of heat exchanger from primary to secondary water in ITER, J. Nucl. Mater. 329–333 (2004) 183–187, https://doi.org/10.1016/j.jnucmat.2004.04.009.
[75] K. Katayama, T. Matsumoto, A. Ipponsugi, Y. Someya, Tritium permeation from tritiated water to water through Inconel, J. Nucl. Mater. 565 (2022) 153723, https://doi.org/10.1016/j.jnucmat.2022.153723.
[76] J. Crank, The Mathematics of Diffusion, 2nd ed, Clarendon Press, Oxford, 1975.
[77] H.T. Lee, E. Markina, Y. Otsuka, Y. Ueda, Deuterium ion-driven permeation in tungsten with different microstructures, Phys. Scr. T (2011), https://doi.org/10.1088/0031-8949/2011/T145/014045.

[78] T. Chikada, H. Fujita, M. Matsunaga, S. Horikoshi, J. Mochizuki, C. Hu, F. Koch, M. Tokitani, Y. Hishinuma, K. Yabuuchi, Y. Oya, Deuterium permeation behavior in iron-irradiated erbium oxide coating, Fusion Eng. Des. 124 (2017) 915–918, https://doi.org/10.1016/j.fusengdes.2017.01.016.
[79] T. Chikada, H. Fujita, J. Engels, A. Houben, J. Mochizuki, S. Horikoshi, M. Matsunaga, M. Tokitani, Y. Hishinuma, S. Kondo, K. Yabuuchi, T. Schwarz-Selinger, T. Terai, Y. Oya, Deuterium permeation behavior and its iron-ion irradiation effect in yttrium oxide coating deposited by magnetron sputtering, J. Nucl. Mater. 511 (2018) 560–566, https://doi.org/10.1016/j.jnucmat.2018.06.008.
[80] P. Muñoz, T. Hernández, I. García-Cortés, F.J. Sánchez, A. Maira, D. Iadicicco, M. Vanazzi, M. Utili, F. Di Fonzo, A. Moroño, Radiation effects on deuterium permeation for PLD alumina coated eurofer steel measured during 1.8 MeV electron irradiation, J. Nucl. Mater. 512 (2018) 118–125, https://doi.org/10.1016/j.jnucmat.2018.10.008.
[81] P. Muñoz, M. Malo, A. Moroño, I. García-Cortés, S. Cabrera, RIPER: an irradiation facility to test Radiation induced Permeation and release of deuterium for fusion blanket materials, Fusion Eng. Des. 145 (2019) 66–71, https://doi.org/10.1016/j.fusengdes.2019.05.004.
[82] H. Fujita, T. Chikada, J. Mochizuki, S. Horikoshi, M. Matsunaga, T. Tanaka, T. Terai, Deuterium permeation through metals under γ-ray irradiation, Fusion Eng. Des. 133 (2018) 95–98, https://doi.org/10.1016/j.fusengdes.2018.04.070.
[83] A. Pisarev, V. Shestakov, S. Kulsartov, A. Vaitonene, Surface effects in diffusion measurements: deuterium permeation through martensitic steel, Phys. Scr. T 94 (2001) 121–127, https://doi.org/10.1238/physica.topical.094a00121.
[84] V. Shestakov, A. Pisarev, V. Sobolev, S. Kulsartov, I. Tazhibaeva, Gas driven deuterium permeation through F82H martensitic steel, J. Nucl. Mater. 307–311 (2002) 1494–1497, https://doi.org/10.1016/S0022-3115(02)01129-7.
[85] E. Serra, P.J. Kelly, D.K. Ross, R.D. Arnell, Alumina sputtered on MANET as an effective deuterium permeation barrier, J. Nucl. Mater. 257 (1998) 194–198, https://doi.org/10.1016/S0022-3115(98)00473-5.
[86] A. Aiello, M. Utili, S. Scalia, G. Coccoluto, Experimental study of efficiency of natural oxide layers for reduction of tritium permeation through Eurofer 97, Fusion Eng. Des. 84 (2009) 385–389, https://doi.org/10.1016/j.fusengdes.2008.12.091.
[87] R.J. Pawelko, M. Shimada, K. Katayama, S. Fukada, P.W. Humrickhouse, T. Terai, Low tritium partial pressure permeation system for mass transport measurement in lead lithium eutectic, Fusion Eng. Des. 102 (2016) 8–13, https://doi.org/10.1016/j.fusengdes.2015.11.005.
[88] J. Mochizuki, S. Horikoshi, H. Fujita, M. Matsunaga, Y. Hishinuma, Y. Oya, T. Chikada, Preparation and characterization of Er2O3-ZrO2 multi-layer coating for tritium permeation barrier by metal organic decomposition, Fusion Eng. Des. 136 (2018) 219–222, https://doi.org/10.1016/j.fusengdes.2018.01.059.
[89] R. Conrad, L. Debarberis, V. Coen, T. Flament, Irradiation of liquid breeder material Pb17Li with in-situ tritium release measurements in the LIBRETTO 2 experiment, J. Nucl. Mater. 179–181 (1991) 875–878, https://doi.org/10.1016/0022-3115(91)90228-Y.
[90] R. Conrad, M.A. Fütterer, L. Giancarli, R. May, A. Perujo, T. Sample, LIBRETTO-3: performance of tritium permeation barriers under irradiation at the HFR Petten, J. Nucl. Mater. 212–215 (1994) 998–1002, https://doi.org/10.1016/0022-3115(94)90984-9.
[91] A.V. Fedorov, S. van Til, A.J. Magielsen, M.P. Stijkel, Tritium permeation in EUROFER in EXOTIC and LIBRETTO irradiation experiments, Fusion Eng. Des. 88 (2013) 2918–2921, https://doi.org/10.1016/j.fusengdes.2013.06.003.
[92] A.V. Fedorov, A.J. Magielsen, M.P. Stijkel, Tritium permeation in EUROFER97 steel in EXOTIC-9/1 irradiation experiment, J. Nucl. Mater. 448 (2014) 139–143, https://doi.org/10.1016/j.jnucmat.2014.01.022.
[93] M. Nakamichi, T.V. Kulsartov, K. Hayashi, S.E. Afanasyev, V.P. Shestakov, Y. V. Chikhray, E.A. Kenzhin, A.N. Kolbaenkov, In-pile tritium permeation through F82H steel with and without a ceramic coating of Cr2O3-SiO2 including CrPO4, Fusion Eng. Des. 82 (2007) 2246–2251, https://doi.org/10.1016/j.fusengdes.2007.05.064.
[94] A. von der Weth, F. Arbeiter, D. Klimenko, V. Pasler, G. Schlindwein, Review of hydrogen isotopes transport parameters and considerations to corresponding experiments, Fusion Eng. Des. 124 (2017) 783–786, https://doi.org/10.1016/j.fusengdes.2017.04.024.
[95] V. Nemanič, B. Zajec, M. Žumer, Sensitivity enhancement in hydrogen permeation measurements, J. Vac. Sci. Technol. A: Vac. Surf. Films 28 (2010) 578–582, https://doi.org/10.1116/1.3442804.
[96] G. Federici, Testing needs for the development and qualification of a breeding blanket for DEMO, Nucl. Fusion 63 (2023) 125002.